

Exploring Non-Gaussian Sea Ice Characteristics via Observing System Simulation Experiments

Christopher Riedel ¹ and Jeffrey Anderson ²

¹Advance Study Program, National Center for Atmospheric Research, Boulder, Colorado

²Data Assimilation Research Section, National Center for Atmospheric Research, Boulder, Colorado

Correspondence: Christopher Riedel (criedel@ucar.edu)

Abstract. The Arctic is warming at a faster rate compared to the globe on average, commonly referred to as Arctic amplification. Sea ice has been linked to Arctic amplification and gathered attention recently due to the decline in summer sea ice extent. Data assimilation (DA) is the act of combining observations with prior forecasts to obtain a more accurate model state. Sea ice poses a unique challenge for DA because sea ice variables have bounded distributions, leading to non-Gaussian distributions. The non-Gaussian nature violates Gaussian assumptions built into DA algorithms. This study presents different observing system simulation experiments (OSSEs), which through experimental observation networks and synthetic observations will provide a data assimilating testing framework. The OSSEs framework will help determine the best data assimilation configuration for assimilating sea ice and snow observations. Findings indicate that assimilating both sea ice thickness and snow depth observations while omitting sea ice concentration observations produced the best sea ice and snow forecasts, in our idealized experimental setup. A simplified DA experiment helped demonstrate that the DA solution is biased when assimilating sea ice concentration observations. The biased DA solution is related to the observation error distribution being a truncated normal distribution, and the assumed observation likelihood is normal for the DA method. Additional OSSEs show that using a non-Gaussian DA method does not alleviate the non-Gaussian effects of sea ice concentration observations, and assimilating sea ice surface temperatures has a positive impact on snow updates. Finally, it is shown that perturbed sea ice model parameters, used to create additional ensemble spread in the free forecasts, lead to a year-long negative snow volume bias.

1 Introduction

Warming over the Arctic region, a phenomenon commonly referred to as Arctic amplification (Serreze and Francis, 2006), has been identified in both observations (Serreze et al., 2009; England et al., 2021) and climate models (Holland and Bitz, 2003). Numerous studies have found this warming rate to be approximately twice as fast as the global average (Walsh, 2014; Jansen et al., 2020; Yu et al., 2021). A recent study found that Arctic amplification-related warming could be three-to-four times faster than the global average, more than double the warming rate previously estimated (Rantanen et al., 2022). Projections of Arctic amplification rely heavily on the ability of coupled numerical models to represent each Earth-system component. One important Earth-system component linked to Arctic amplification—the cryosphere—has gathered attention recently due to the declining summer sea ice extent over the recent decades (Screen and Simmonds, 2010; Jenkins and Dai, 2021). During wintertime, sea

25 ice can act as an insulator trapping ocean heat, created from the absorbed shortwave radiation during the summer sea-ice loss season, within the ocean allowing for cooler winter atmospheric temperatures (Chung et al., 2021). Additionally, snow cover on top of sea ice can impact seasonal sea ice evolution, growth and melt (Holland et al., 2021). Providing more accurate sea ice and snow states via data assimilation in our coupled Earth-system modeling frameworks could help improve future projections of the climate and the processes related to Arctic amplification.

30 Data assimilation (DA) is the action of optimally combining information from prior forecasts with observations to improve the current estimate of the state of any Earth-system component. The statistical methods used to optimally combine this information often have Gaussianity assumptions, depending on the choice of the data assimilation method. One data assimilation method that has commonly been applied in Earth-system problems is the ensemble Kalman filter (EnKF; Evensen 2003; Houtekamer and Zhang 2016), which includes Gaussian assumptions in its original Kalman filter formulation (Kalman, 1960).
35 These Gaussian assumptions can lead to biased solutions when prior forecast distributions are non-Gaussian or errors associated with the observations are also non-Gaussian. Common sea ice variables have both double and single bounded quantities (e.g., doubly-bounded: sea ice concentration; singly-bounded: sea ice thickness) that lead to non-Gaussian distributions, which would violate Gaussian assumptions. Studies have investigated the performance of different EnKF formulations (stochastic versus deterministic) under non-Gaussian conditions and found that while the stochastic formulation was more stable, both had
40 biased solutions (Lawson and Hansen, 2004; Lei et al., 2010). Different ensemble data assimilation methods that remove the Gaussian assumption have been proposed, however, many have only been tested in low-order models and could be potentially expensive in high-dimensional geophysical models (Pham, 2001; Anderson, 2010; Sakov et al., 2012b; Metref et al., 2014). Here, instead of testing a new ensemble data assimilation method, we will conduct experiments to highlight the impacts of different non-Gaussian sea ice variables during data assimilation updates.

45 The application of data assimilation to sea ice problems is not a novel idea since this research topic has been investigated for more than two decades. Common observation descriptive quantities for sea ice are concentration (e.g., the fraction of a grid cell covered with sea ice) and thickness (e.g., the sea ice surface extending down into the ocean). Previous studies have highlighted the importance of initial conditions when trying to predict Arctic sea ice from local to seasonal time scales, especially regarding accurate initialization of sea ice thickness (Msadek et al., 2014; Day et al., 2014; Dirkson et al., 2017). Although different data
50 assimilation techniques have been used to update sea ice state variables (Meier and Maslanik, 2003; Van Woert et al., 2004; Lindsay and Zhang, 2006; Stark et al., 2008), numerous studies have tested updating sea ice state variables using the EnKF data assimilation method (Lisæter et al., 2003; Barth et al., 2015). These EnKF studies were tested both in a synthetic observation framework referred to as observing system simulation experiments (OSSEs; Barth et al. 2015; Kimmritz et al. 2018; Zhang et al. 2018) and using real observations from remote sensing platforms (Sakov et al., 2012a; Massonnet et al., 2015). These studies
55 found improvements in both sea ice analyses and their corresponding forecasts related to the spatial sea ice concentration field but little improvement in sea ice thickness. In addition, studies have improved the initialization of sea ice cover when updating sea ice thickness via a multivariate framework when assimilating only sea ice concentration observations (Massonnet et al., 2015; Sakov et al., 2012a). More recent studies have tested the assimilation of sea ice thickness observations and found further improvements to both sea ice thickness and sea ice concentration states (Mathiot et al., 2012; Chen et al., 2017; Fritzner et al.,

60 2018; Mu et al., 2018; Fiedler et al., 2022). While results from assimilating sea ice thickness observations are positive, they contain large observation uncertainties because satellite remote sensing retrieval algorithms contain large uncertainties due to input parameters and instrument errors (Kwok and Cunningham, 2008; Zygmuntowska et al., 2014; Tilling et al., 2016; Xie et al., 2016; Ricker et al., 2017). Further research is needed to determine how to properly handle these uncertainties when assimilating sea ice observations. Lastly, there have been recent attempts to obtain observed snow depth from satellites; 65 however, the uncertainties associated with these observations remain high (Maaß et al., 2013; Rostosky et al., 2018). Because snow is closely connected to albedo and sea ice melting, further understanding of the impacts of assimilating snow depth observations is needed. For example, Fritzner et al. 2019 found assimilating snow depth observations had positive effects on short-term forecasts of snow depth and sea ice concentration.

This study uses different OSSEs to investigate how the non-Gaussian nature of different sea ice fields impacts data assimilation- 70 generated sea ice analyses. Using OSSEs provides an experimental framework to test the impacts of synthetically generated observations in different data assimilation configurations. This study expands on previous research on sea ice data assimilation that was laid out by Zhang et al. (2018). The OSSEs presented in this study will test different experimental setups to investigate their impacts on sea ice and snow states generated by data assimilation. These experiments will investigate the impacts of post-processing updates for snow on top of sea ice, different assimilated observation combinations, and different data assimilation 75 methods. This study highlights the impacts of the non-Gaussian nature of certain sea ice variables on the generation of sea ice analyses when using an EnKF data assimilation method. Section 2 describes the sea ice model and the data assimilation experimental setup along with the description of the different OSSEs that were completed. Section 3 presents the results obtained from the different OSSEs. Section 4 discusses the conclusions and future work on this research.

2 Methods and Experimental Setup

80 2.1 DART-CICE data assimilation system

For this study, the Los Alamos Sea Ice Model version 5 (CICE5; Hunke et al. 2015) is used to integrate the analyses forward in time while using an ensemble Kalman filter (EnKF) data assimilation technique to generate analyses. The Data Assimilation Research Testbed (DART; Anderson et al. 2009) software was used to implement the EnKF. Hereafter, we refer to this modeling configuration as CICE-DART. The CICE5 model setup closely follows that in Zhang et al. (2018) while the data assimilation 85 setting will be different in the experiments.

2.1.1 DART

The data assimilation technique used in this study is the ensemble adjustment Kalman filter (EAKF; Anderson 2001), which is a modified version of the ensemble Kalman filter (Burgers et al., 1998) and a variation of the deterministic ensemble square-root filter (Tippett et al., 2003). The EAKF combines observations with an ensemble of short-term model forecasts over a 90 specific observation window to produce an ensemble of the best estimate of the sea ice state. One important aspect of the

EAKF is its ability to use the ensemble to estimate a flow-dependent background-error covariance, which differs from a static background-error covariance typically employed by variational techniques. Additionally, a non-Gaussian rank histogram filter (RHF, filter option 8 in DART; Anderson 2010) is tested to compare with EAKF results. To reduce sampling errors due to limited ensemble member size, covariance localization was applied only in the horizontal direction. A Gaspri-Cohn fifth-order polynomial was applied in the horizontal directions to limit observation updates within a specified cutoff radius of 0.05 (i.e., ~320 km; Gaspari and Cohn 1999). Adaptive prior covariance inflation was applied by “inflating” the ensemble perturbations in prior background fields, increasing the variance by pushing ensemble members away from the ensemble mean (Anderson, 2007). Zhang et al. (2018) found a reduction in Arctic sea ice area and volume errors when prior inflation was applied in their study. Inflation damping is set to 0.9 to help control the growth of the inflation factor for the different state model variables. Any assimilated observation type is allowed to update all model state variables during the assimilation step unless otherwise noted. There was no cross-variable localization applied in this study.

2.1.2 CICE

CICE5 is the sea ice component within the Community Earth System Model (CESM; Danabasoglu et al. 2020) that is used to make climate projections. CICE5 simulates the evolution of sea ice and snow through the representation of thermodynamic and dynamical processes using an ice thickness distribution. The evolution of sea ice thickness, which is represented by the quotient of sea ice volume and sea ice area, is accomplished by partitioning the sea ice pack distribution within a grid cell into multiple thickness categories (Lipscomb, 2001). For this study, there are five thickness categories for both sea ice and snow with lower bounds of 0, 0.64, 1.39, 2.47, 4.57 m. Respecting the category bounds poses a challenge during the data assimilation step when updating sea ice area and sea ice volume. Snow depth is also partitioned into five categories. Each thickness category is divided into multiple layers (both sea ice and snow if present) to represent the evolution of sea ice temperature, salinity, and enthalpy related to sea ice and snow. CICE was coupled to a slab ocean model (SOM) that provides the ocean forcing in the form of annually periodic, prescribed ocean forcing data (e.g., sea surface temperatures, ocean heat fluxes). The atmospheric forcing data comes from the Community Atmosphere Model version 6 (CAM6)/Data Assimilation Research Testbed ensemble reanalysis (Raeder et al., 2021) for the time period of interest. Default namelist settings were used in this study (Hunke et al., 2015) except for perturbing several input CICE parameters, which will be discussed in the next section.

2.2 Perfect model OSSEs

Given the uncertainties and potential biases of satellite-retrieved sea ice and snow observations, this study applies perfect model OSSEs to investigate non-Gaussian impacts that could be introduced while assimilating these observations. Each ensemble consists of 80 CICE5 members because there are 80 different CAM6/DART reanalysis atmospheric forcing files. Each CICE5 ensemble member uses the same SOM forcing. To increase the ensemble spread, three different parameters were perturbed that impact albedo, heat transfer through snow, and the ability to move sea ice within the ocean. The standard deviation of the dry snow grain radius (R_{snw}) controls the optical properties of snow and is one of the key parameters that determines snow albedo in the solar radiation parameterization (Briegleb and Light, 2007). The thermal conductivity of snow (k_{snw}) directly impacts the

amount of heat that can be transferred through the snow pack, thereby affecting the evolution of sea ice (Sturm and Massom, 2017). The neutral ocean-ice drag coefficient (dragio) controls the horizontal momentum exchange at the ice-ocean interfaces, which determines the drag forces on the sea ice (Lu et al., 2011). These three parameters were chosen because they are among the top parameters that drive variability within CICE5 in both summer and winter (Urrego-Blanco et al., 2016). See the data availability statement for access to the perturbed parameter values used in this study. To achieve the climatological state of sea ice and snow, a single member is run for 40 years using periodic atmospheric forcing for the year 2012. To build our 80 member ensemble, we first used only 80 different atmospheric forcings to cycle over 2012 for 10 years to build in variability related to the atmosphere. Each ensemble member is then run for an additional 15 years, cycling over 2012, using the distinct atmospheric forcing and parameter set to generate free forecasts that can be used as a reference case (Fig. 1). One of the free forecast members is randomly chosen as the simulated “truth.” For this study, the free forecast ensemble mean is negatively biased compared to the truth member for different sea ice and snow characteristics. The free forecasts will provide a reference for comparison with the different data assimilation experiments.

Since satellites can not retrieve multi-category model quantities, aggregate synthetic observations are generated from the truth member to produce sea ice concentration (SIC), sea ice thickness (SIT), snow depth (D_{snow}), and sea ice surface temperature (SIST). The multi-category state model variables that are updated via data assimilation or post-processing are sea ice area ($A_{\text{ice},n}$), sea ice volume ($V_{\text{ice},n}$), and snow volume ($V_{\text{snow},n}$). When those multi-category state model variables are summed over the different categories, they are referred to as A_{ice} , V_{ice} , and V_{snow} . To compute data assimilation updates, it is necessary to compute an observation’s expected value from the model state, which is called the forward operator. SIC is just the sum of the area values in the different thickness categories computed as

$$\text{SIC} = \sum_{n=1,5} A_{\text{ice},n}. \quad (1)$$

The mean SIT of a grid cell is computed by summing the sea ice volumes in the different thickness categories and then dividing by the aggregated sea ice area as follows

$$\text{SIT} = \frac{\sum_{n=1,5} V_{\text{ice},n}}{\sum_{n=1,5} A_{\text{ice},n}}. \quad (2)$$

The mean D_{snow} of a grid cell is computed in the same fashion as SIT except using summed snow volumes

$$D_{\text{snow}} = \frac{\sum_{n=1,5} V_{\text{snow},n}}{\sum_{n=1,5} A_{\text{ice},n}}. \quad (3)$$

The mean SIST of a grid cell is the area weighted mean temperature across the different thickness categories on the surface of the sea ice

$$\text{SIST} = \frac{\sum_{n=1,5} \text{SIST}_n * A_{\text{ice},n}}{\sum_{n=1,5} A_{\text{ice},n}} \quad (4)$$

where SIST_n is the sea ice surface temperature for the different thickness categories. In this OSSE framework, synthetic observations are generated from the truth member using the forward operators and are assimilated. Normally, synthetic observations

are created by adding a draw from a normal distribution with a mean of zero and a specified observation error standard deviation. This method was chosen to create the synthetic sea ice surface temperature observations that were assimilated. However, sea ice and snow quantities have single (SIT, D_{snow}) and double (SIC) bounds in their representations. Because of this, we will use a single (SIT, D_{snow}) and double (SIC) truncated normal distribution when generating the synthetic sea ice and snow observations that are assimilated in our OSSEs. The observation error standard deviation for SIC is 15% of the true values of SIC ($\text{SIC}_{\text{error}} = \text{SIC}_{\text{truth}} * 0.15$; Zhang et al. 2018) and 0.1 m for SIT (approximation of future high precision data; Zhang et al. 2018). While studies that use real SIT observations have varied their uncertainties depending on the thickness value (Xie et al., 2018; Cheng et al., 2023), due to the complexity of computing SIT (Zygmuntowska et al., 2014) this study chose to use a single value for SIT uncertainty. The SIT observation error of 0.1 m is a goal for future satellite platforms and is not the observation error for current observing platforms. The observation error standard deviation is 10% of the true values of D_{snow} (approximation of future high precision data; Rostosky et al. 2020) and 1.5°C for SIST (Hall et al., 2015). Due to the SIC observation error method, only synthetic SIC observations greater than 0.01 (approximately the precision found in passive microwave sea ice concentration observation files, Meier et al. 2021) are assimilated. Similarly, the observation error for D_{snow} has a lower bound of 0.005 m for synthetic observations close to zero. The locations for all synthetic observation types that are assimilated were based on CryoSat-2 locations (locations measured every 10 seconds; more details on locations see CryoSat-2 Product Handbook at <https://earth.esa.int/eogateway/documents/20142/37627/CryoSat-Baseline-D-Product-Handbook.pdf>), which provides the observational network for testing (Fig. 2). While different sea ice observation networks in the real world usually do not match, the observation network chosen for this study was chosen because of the easy experimental setup and fair comparison between the synthetic observations that were assimilated in this study.

Six different experiments were completed to test different observation combinations, data assimilation techniques, and post-processing updates (Table 1). EAKF-ConcThick is an extension of the work completed by Zhang et al. (2018) where they only allowed observation increments to update the sea ice area in the different categories while updating the sea ice and snow volume via post-processing. In EAKF-ConcThick, we allow the category-based sea ice area and volume to be updated independently by synthetic SIC and SIT observations while updating snow volume via post-processing. The equations for post-processing snow volume updates in the different categories are the following:

$$h_{\text{snow},n}^{\text{prior}} = \frac{V_{\text{snow},n}^{\text{prior}}}{A_{\text{snow},n}^{\text{prior}}}, \quad (5)$$

180

$$V_{\text{snow},n}^{\text{posterior}} = A_{\text{ice},n}^{\text{posterior}} \times h_{\text{snow},n}^{\text{prior}}, \quad (6)$$

where $A_{\text{ice},n}^{\text{prior}}$ is the prior sea ice area in the different thickness categories, $V_{\text{snow},n}^{\text{prior}}$ is the prior snow volume in the different thickness categories, $A_{\text{ice},n}^{\text{posterior}}$ is data assimilation updated sea ice area in the different categories and $h_{\text{snow},n}^{\text{prior}}$ are the prior snow thickness values in the different categories. In EAKF-ConcThickSnow, snow volume is no longer updated by post processing and assimilation of synthetic D_{snow} is included in the assimilated observation subset. Since real world snow depth observations still have their limitations (Rostosky et al., 2018; Fritzner et al., 2019), the synthetic snow depth observations generated for this

OSSE will test the impacts if high-quality snow observations are available year-round in the future. All assimilated synthetic observations (SIC,SIT,SNWD) update all category-based model state variables ($A_{ice,n}, V_{ice,n}, V_{snow,n}$). To test the non-Gaussian effects of the synthetic SIC observations, EAKF-ThickSnow only assimilates synthetic SIT and D_{snow} while allowing the category-based sea ice area, sea ice volume, and snow volume state variables to be updated from the observation increments. RHF-ConcThickSnow investigates the impacts of using a non-Gaussian data assimilation method, the rank histogram filter, when working with the non-Gaussian sea ice and snow variables in the CICE model. EAKF-ModifiedFO investigates the impacts of having sea ice thickness and snow depth output from CICE instead of having the forward operators within DART compute these quantities. This arises from the fact that prior inflation is applied, which can push either the sea ice area or sea ice volume below zero. Since computing sea ice thickness or snow depth is the division of either sea ice or snow volume by the sea ice area, this could lead to shuffling of the distribution if values become negative. Finally, EAKF-SIST tests the impacts of assimilating additional synthetic SIST observations to further improve the updates of sea ice and snow states. While synthetic SIST observations are assimilated, sea ice surface temperatures in the different thickness categories are not updated from the data assimilation step.

Due to the bounds related to sea ice and snow state variables, there are different conditions under which special treatment is needed to ensure that the respected bounds are met. SIC (summed sea ice area across the categories) must remain between 0 and 1. Similarly, sea ice and snow volumes (summed across the categories) must remain above zero. If negative values occur for SIC or the volumes, all categories are set to zero. Additionally, category-based sea ice area values are scaled if the SIC exceeds one after the assimilation updates. In the event SIC exceeds one, the scaling of the category-based sea ice area is as follow:

$$A_{ice,n} = A_{ice,n} * \frac{1}{SIC}. \quad (7)$$

In the case where SIC is within the bounds but individual categories become negative, those categories are set to zero and the remaining nonzero categories are reduced proportionally to compensate for the negative amount. Lastly, special care is taken to account for the cases where SIC is greater than zero but sea ice volume in all categories is zero. This can occur during data assimilation updates to the category-based sea ice volume (updates removes all the sea ice volume) or if the data assimilation updates create some amount of sea ice area but the sea ice volume remains zero. A new sea ice volume is computed by multiplying the average thickness value allowed in the associated category (0.32, 1.01, 1.93, 3.51, 6.95) by the sea ice area for the category.

The same initial conditions used to generate the free forecasts were used for the experiments listed in Table 1. The free forecasts provide a reference to the amount of variability that was generated during the spin-up process (Fig. 1). All experiments were initialized on 1 January 2013 and the cycling period was for the entire year 2013. In all experiments, observations were assimilated at a daily interval.

2.3 Model Verification Metrics

Time series of total sea ice area, sea ice volume, and snow volume will be ensemble mean forecast quantities used to evaluate
 220 CICE-DART performance over the cycling period. The equations for computing total sea ice area and volume are as follows:

$$\text{Total-Sea-Ice-Area}(t) = \sum_{n=1,j} (\text{SIC}(t)_j * \text{grid-cell-area}_j), \quad (8)$$

$$\text{Total-Sea-Ice-Volume}(t) = \sum_{n=1,j} (\text{V}_{\text{ice}}(t)_j * \text{grid-cell-area}_j), \quad (9)$$

where t is time, j is the total number of grid points in the Northern Hemisphere and grid-cell-area is the area of the grid cell.
 225 Total snow volume is computed in the same way as total sea ice volume but instead using snow volume. Spatial Probability Score (SPS) is computed to investigate potential sea ice edge errors over the cycling period (Goessling and Jung, 2018). Following Goessling and Jung 2018, the ice edge is defined using the 15% sea ice concentration contour in this study. Due to data storage issues, SPS could not be calculated for EAKF-SIST. Additionally, ensemble mean spatial biases will be computed for SIC, sea ice volume, and snow volume over different cycling periods. Welch's t-test will be applied to test for significant
 230 biases (Welch, 1947). The ensemble mean was chosen because the statistics were nearly identical regardless of whether the ensemble mean or ensemble median was used.

Mean absolute bias (MAB) and mean square error (MSE) will be computed over the time series of total sea ice area, sea ice volume, and snow volume for additional performance evaluation. The equations for MAB and MSE are as follows:

$$\text{MAB} = \sum_{t=1}^N |X_i^m - X_i^t|, \quad (10)$$

235

$$\text{MSE} = \sum_{t=1}^N (X_i^m - X_i^t)^2, \quad (11)$$

where i is the time index, N is the total number of times (i.e, number of days), X_i^m ensemble mean forecast quantity (e.g., total sea ice area), and X_i^t is the true value for the forecast quantity. The integrated ice-edge error (IIEE) is another forecast metric that is applied to the ensemble mean, which is analogous to SPS when using a single, deterministic forecast (Goessling et al.,
 240 2016). IIEE evaluates potential sea ice edge differences between the ensemble mean and the truth. IIEE is more suitable for user forecast evaluation of the sea ice edge compared to the traditional sea ice extent (Tietsche et al., 2014). The IIEE is the sum of the area grid boxes where the ensemble mean and the truth disagree on whether sea ice is present (over-prediction; $\text{SIC}_{\text{truth}}=0$ and $\text{SIC}_{\text{ensemble mean}}>0$) or not (under-prediction, $\text{SIC}_{\text{truth}}>0$ and $\text{SIC}_{\text{ensemble mean}}=0$). Similar to previous studies computing IIEE, a SIC threshold of 15% is used to determine whether a grid cell is identified as having sea ice (Goessling and Jung,
 245 2018; Zampieri et al., 2018). An attractive feature of IIEE is that it can be decomposed into an absolute extent error (AEE) and a misplacement error (ME). AEE is the absolute difference ($|\text{over-prediction} - \text{under-prediction}|$) between predictions, which

can help determine whether there is a bias for over- or under-predicting sea ice coverage. MEE is the misplacement error ($2 \times \min(\text{over-prediction}, \text{under-prediction})$) reflecting whether there is too much sea ice in one location and too little in another. IIEE along with its components AEE and ME will be computed daily. Welch's t-test was used to determine whether there were significant differences between MAB, MSE, and IIEE values between experiments. Finally, Spearman correlations are computed between the perturbed parameters and different CICE model outputs.

3 Results and discussion

3.1 Optimization of sea ice and snow data assimilation

The first three experiments investigate which assimilated synthetic observation subset produces the most accurate forecasts for both sea ice and snow. All the experiments have similar skill in predicting the sea ice edge and are better than the free forecast (Fig. 3A). However, there is a period during August and September when experiments assimilating SIC, EAKF-ConcThick and EAKF-ConcThickSnow, have smaller errors in predicting the sea ice edge. Daily biases of total sea ice area, sea ice volume, and snow volume are computed throughout the cycling period to compare the performance of the experiments with the truth and free forecasts (Fig. 3B,C,D). Compared with the free forecast, EAKF-ConcThick performs better for both total sea ice area and sea ice volume. However, total sea ice area and sea ice volume were negatively biased from the start of the melt season in May until the re-freeze in September. Total snow volume for EAKF-ConcThick is comparable to the free forecasts. This means that the post-processing updates for the snow state variable are not as accurate compared to the sea ice state variables, which are updated directly from the multivariate data assimilation step. For EAKF-ConcThickSnow, there is little impact on biases associated with sea ice quantities. The biases associated with total snow volume are reduced in the EAKF-ConcThickSnow compared to EAKF-ConcThick and the free forecasts. This highlights the potential impacts snow depth observations could have if assimilated year-round which due to limitations is not possible (Rostosky et al., 2018). The negative biases found for total sea ice and sea ice volume during the summer for the first two experiments are now near zero for EAKF-ThickSnow. Improvements in total snow volume for EAKF-ThickSnow are isolated to the start of the melt season, however, the biases are similar to the first two experiments after this period. Regardless of these improvements, total snow volume is negatively biased throughout the cycling period for experiments where D_{snow} observations are assimilated. Additionally, the biases for total snow volume are larger during the winter seasons leading up to June and then approach zero thereafter for experiments where D_{snow} observations are assimilated. This result could mean that it takes a seasonal cycle to pull ensemble snow values closer to the truth. Removing SIC observations from the assimilated observation subset eliminates an observation that is doubly-bounded and whose values approach both of the bounds. Since SIC observations are more likely to be affected by their associated bounds (bulk of SIC observations near 1 unless near marginal ice zone) this could be the driving factor for the poor forecasts in the first two experiments.

Temporal forecast metrics are computed over the cycling period to pin-point which experiment is more accurate (Fig. 4). EAKF-ConcThick and EAKF-ConcThickSnow have the lowest total IIEE and are significantly different from the free forecast and EAKF-ThickSnow. This means that both EAKF-ConcThick and EAKF-ConcThickSnow produce a more accurate forecast

280 of sea ice coverage over the cycling period. This might seem inconsistent since the EAKF-ThickSnow daily biases were smaller. EAKF-ThickSnow has sea ice area MSE and MAB that is lower and significantly different from the other experiments and the free forecast. This means that removing the SIC observations provided a more accurate forecast of the sea ice area, however, this did have a negative impact on predicting the sea ice edge in EAKF-ThickSnow. This indicates that SIC observations play an important role in maintaining the sea ice edge close to the truth. Additionally, all experiments performed better for sea ice
285 volume compared with the free forecast, with EAKF-ThickSnow being the most accurate. For snow volume, EAKF-ConcThick is not statistically better than the free forecast, indicating that post-processing snow updates is not a favorable method. Once again, EAKF-ThickSnow performs the best for snow volume even though SIC observations are not assimilated. While not assimilating SIC observations improves most forecast metrics, these observations are crucial for accurately representing the sea ice edge.

290 While EAKF-ThickSnow provided the most accurate forecasts for aggregated quantities, such as total sea ice area, it is unclear where those improvements occurred spatially over the Arctic at the start of the melt season. To gain more insight into the improved results, May-through-June averaged spatial biases of SIC, V_{ice} and V_{snow} are computed for the free forecast and each of the first three experiments (Fig. 5). For SIC, there are significant biases for the free forecast where the SIC values are too large over the central Arctic and too small near the marginal ice zone. EAKF-ConcThick and EAKF-ConcThickSnow show
295 predominantly significant negative biases over the sea ice for SIC, whereas EAKF-ThickSnow reduces the spatial biases to near zero. The negative SIC spatial bias over the central Arctic explains why the total sea ice area for EAKF-ConcThick and EAKF-ConcThickSnow performed poorly compared to EAKF-ThickSnow. However, there are areas of larger bias value near the marginal ice zone for EAKF-ThickSnow, meaning it was less accurate in representing the sea ice edge. While all experiments reduced the magnitude of the V_{ice} spatial bias, there is still an overall significant negative bias for EAKF-ConcThick and EAKF-
300 ConcThickSnow. The spatial biases for EAKF-ThickSnow are near zero, and there are essentially no areas of significant bias. For V_{snow} , there are differences between the spatial biases for EAKF-ConcThick and EAKF-ConcThickSnow, highlighting the benefits of assimilating D_{snow} observation over post-processing V_{snow} updates. In EAKF-ThickSnow, there is an overall reduction in the significant negative biases over the central Arctic compared with EAKF-ConcThickSnow. In EAKF-ConcThick and EAKF-ConcThickSnow, the SIC observations have a negative impact on both the observed and non-observed model state
305 variables. Removing SIC observations from the assimilated observation subset reduced the spatial coverage of significant biases for all state model variables.

An analysis increment indicates how the observations are pushing or pulling state model variables. Evaluating analysis increments will help determine how the assimilation of synthetic SIC observations impact the different data assimilation experiments. For EAKF-ThickSnow, there is a reduction in the magnitude of the spatial analysis increments at the start of the melt
310 season compared with EAKF-ConcThick and EAKF-ConcThickSnow (Fig. 6A). The analysis increment reduction is mainly located over the central part of the Arctic, where SIC values for all ensemble members are close to 1. This implies that the assimilation of SIC observations leads to low biased SIC analyses. The SIC analysis increments become more similar across the experiments as one moves away from the central Arctic toward the marginal ice zone. The analysis increment patterns and magnitudes near the marginal ice zone for EAKF-ConcThick are less different than one might expect because of the increase

315 in IIEE. However, these analysis increments are averaged from May through June; therefore, the IIEE might be picking up
on sea ice edge errors at different times throughout the cycling period. This is similar for the V_{ice} , where there is a reduc-
tion in the analysis increment magnitude over the central Arctic for EAKF-ThickSnow compared with EAKF-ConcThick and
EAKF-ConcThickSnow (Fig. 6B). For V_{snow} analysis increments, there is a flip in the sign between EAKF-ConcThick and
EAKF-ConcThickSnow (Fig. 6). The negative V_{snow} analysis increments in EAKF-ConcThick are connected to the SIC analy-
320 sis increments due to the equation for post-processing (Equations 5 and 6). Since SIC analysis increments are mainly negative
over the central Arctic, this would also lead to negative V_{snow} analysis increments over this region due to the post-processing
method. The differences in V_{snow} analysis increments between EAKF-ConcThickSnow and EAKF-ThickSnow are small, indi-
cating that the removal of synthetic SIC observations from the assimilated subset does not have a negative impact on the
adjustments. Overall, EAKF-ThickSnow provides the best setup for sea ice and snow data assimilation. Even with a slightly
325 higher IIEE, the removal of the synthetic SIC observations from the assimilate observation subset did provide better results.
Further investigation is needed to understand the reason behind the persistent negatively biased total snow volume compared
to the truth.

3.2 Further discussion on sea ice data assimilation

The removal of SIC as an assimilated synthetic observation improved forecasts of total sea ice, however, forecasts of the
330 sea ice edge were less accurate according to the total IIEE and SPS. This result indicates that near the marginal ice zone
there are benefits to assimilating SIC observations and that SIT observations provide poor multivariate updates for $A_{ice,n}$.
Three additional experiments were completed to investigate the impacts on sea ice when using a non-Gaussian RHF, modified
forward operators for synthetic thickness observations, and the assimilation of synthetic SISTs. Each additional experiment is
compared with EAKF-ThickSnow. Sea ice edge errors are lower in RHF-ConcThickSnow, and the errors are larger in EAKF-
335 ModifiedFO compared with EAKF-ThickSnow (Fig. 7A). Once again, this result highlights improvements when assimilating
SIC observations near the sea ice edge. RHF-ConcThickSnow performs worse than EAKF-ThickSnow during the summer
according to daily biases of total sea ice area, sea ice volume, and snow volume (Fig. 7B,C,D). The use of the non-Gaussian
RHF did not handle the SIC observations better. Compared to EAKF-ThickSnow, EAKF-ModifiedFO and EAKF-SIST have
similar daily biases for total sea ice and snow volume, however, not for total sea ice area. EAKF-ModifiedFO and EAKF-
340 SIST have persistent, larger daily biases during summer compared to EAKF-ThickSnow. There does appear to be a slight
improvement in total snow volume for EAKF-SIST compared with EAKF-ThickSnow during May, however, there are still
negative biases throughout the cycling period.

RHF-ConcThickSnow does the best job representing sea ice coverage since its total IIEE is the lowest and it is significantly
different from the other experiments (Fig. 8). RHF-ConcThickSnow assimilates SIC observations, which is likely why it is
345 similar to our previous result from EAKF-ConcThickSnow (compare Fig. 4A with Fig. 8A). EAKF-ModifiedFO and EAKF-
SIST essentially have the same total IIEE, which is statistically worse than EAKF-ThickSnow. The modification of the forward
operator along with assimilating SIST observations does not improve the representation of sea ice coverage. For total sea
ice area and sea ice volume, RHF-ConcThickSnow has the largest aggregated errors that are significantly different from the

other experiments (Fig 8B, C). This result is similar to EAKF-ConcThickSnow, where SIC observations were assimilated. While EAKF-ThickSnow does the best job representing the total sea ice area and sea ice volume, one thing that needs to be mentioned is that EAKF-SIST uses a modified forward operator. Since the sea ice statistics appear very similar between EAKF-ModifiedFO and EAKF-SIST, the modified forward operator could explain why the results for EAKF-SIST are worse than those for EAKF-ThickSnow.

Evaluating SIC over the start of the melt season (May-through-June) reveals that RHF-ConcThickSnow mostly has significant negative biases compared to the truth (Fig. 9A). This result is similar to EAKF-ConcThickSnow, where the EAKF is used instead of the RHF. Compared to EAKF-ThickSnow, there are larger, positive SIC biases for EAKF-ModifiedFO and EAKF-SIST near the marginal ice zone. These biased areas are mainly located in the Baffin Bay, Greenland Sea, and Barents Sea. The poor representation of the marginal ice zone for EAKF-ModifiedFO and EAKF-SIST could explain the larger total IIEE compared to EAKF-ThickSnow. RHF-ConcThickSnow has significant negative sea ice volume biases over most of the sea ice pack (Fig. 9B). Again, this agrees with the spatial biases for EAKF-ConcThickSnow over this period, further showing that switching to the RHF over the EAKF did not help alleviate the impacts of the SIC observations. The spatial biases of sea ice volume for EAKF-ModifiedFO and EAKF-SIST closely resemble those found in EAKF-ThickSnow, except near the marginal ice zone. The modified forward operator might introduce poor marginal ice zone updates without the constraint of SIC observations in this region. Overall, switching the data assimilation filter type did not resolve the issues related to assimilating SIC observations, and there are potential issues with using the modified forward operator near the marginal ice zone. However, the spatial biases are similar over most of the central Arctic, indicating that further investigation is needed to determine the negative impacts of the modified forward operator.

3.3 Simplified Data Assimilation Experiment

To further investigate the poor results obtained when assimilating SIC observations, a simplified data assimilation experiment was setup. This simplified DA experiment mimics SIC during wintertime over the pole, meaning that the true SIC does not change over time. With a constant truth value that does not change, synthetic observations are created that will be assimilated over the cycling period. The true SIC value is set to 0.99, and its corresponding observation error will vary from 0.1485 (value if using the same method as the OSSE experiments), 0.07425, and 0.037125. Two different filters, EAKF and RHF, will be tested using different observation error specifications. The initial ensemble spread has a standard deviation of 0.0142. No prior inflation was applied in these experiments. Six mini experiments were completed using a combination of different filter types (EAKF or RHF) and different specified observation errors. The experiments were cycled 5,000 times, assimilating the synthetic observations generated from the truth using a truncated normal distribution. These experiments will work with SIC directly, meaning that there are no thickness categories as in CICE. This means that the mapping between observation space to state space is linear, further simplifying this data assimilation experiment.

For all experiments, the prior ensemble mean drifts away from the true value and moves toward the average observation value over the cycling period (Fig. 10). The average observation value depends on the observation error specification; a smaller error leads to an average observation closer to the truth. For the largest observation error, the EAKF drifts toward the average

observation value at a quicker rate compared with the RHF (Fig. 10A,D). The slower rate exhibited by the RHF could mean that the filter weights the observations less compared with the EAKF. Even as the observation errors decrease, both the EAKF and the RHF move away from the truth and drift toward the average observation value (Fig. 10B,C,E,F). These experiments highlight that a reduction in the observation error still results in the prior ensemble being negatively biased when using distributions and observations near a bound.

The fact that the prior ensemble mean moves away from the true value regardless of filter type and observation error value demonstrates that our data assimilation solution is biased. This is because our observation error distribution is a truncated normal, whereas the observation likelihood for EAKF and RHF is assumed to be normal. Applying a non-Gaussian distribution for observation errors while using a Gaussian observation likelihood can lead to erroneous observation impacts, biasing analysis estimates (Pires et al., 2010; Fowler and Jan Van Leeuwen, 2013). This negative bias is exacerbated by the effects of prior inflation in our OSSEs by increasing prior variance, which further weights the observations even more. A better choice might be a combination of distributions representing the prior state and the observation errors more appropriately, as laid out in Anderson (2022).

3.4 Further discussion on snow data assimilation

Regardless of the first three experiments, the daily biases for snow volume are negative throughout much of the entire cycling period compared to the truth (Figs. 3D). Even the daily biases for the additional experiments are mainly negative throughout the cycling period (Fig. 7D). Further investigation is needed to fully understand why the snow volume is negatively biased regardless of the experimental setup. EAKF-ThickSnow will be further evaluated to investigate the reason for the low bias in snow volume. Since the ocean forcing is the same across ensemble members, the atmospheric forcing is evaluated for the ensemble mean. Breaking down the individual atmospheric heat fluxes, the shortwave radiation has the largest bias compared to the truth (Fig. 11A). The other atmospheric heat fluxes have smaller and near zero biases for most of the cycling period. The positive shortwave heat flux bias occurs during sunrise over the Arctic, which also corresponds to the period in EAKF-ThickSnow where the daily biases for snow volume are the largest (Fig. 3C). The spread in the absorbed shortwave heat flux grows during the onset into summer, which is during the start of the snow melt season (Fig. 11B). On average, the ensemble has absorbed too much incoming shortwave radiation compared to the truth. Interestingly, the spread of the absorbed shortwave heat flux collapses at the start of July, when the snow on top of the sea ice is at its minimum (Fig. 3C). One feature that can impact the absorbed shortwave radiation and is connected to snow cover is surface albedo (Fig. 11C). During the same period, the spread in the absorbed shortwave heat flux increases and the spread in the surface albedo spread increases. The spread in the surface albedo then collapses, similar to the incoming shortwave radiation heat flux, near the beginning of July. The surface albedo is, on average, too small compared to the truth, which could be the reason for the positive bias in the absorbed shortwave radiation. Lastly, the ensemble members almost appear to be sorted for both absorbed shortwave radiation and mean surface albedo, hinting that something systematic drives these quantities.

One potential reason that could be driving the negative biases found for the ensemble mean snow volume is that the snowfall originating from the atmospheric forcing file for the truth member is an outlier. This does not appear to be the case when

comparing daily biases of snowfall with the ensemble mean (Fig. 11D). The snowfall biases for the ensemble mean are near zero and fluctuate about the zero line, indicating that there is no clear systematic difference from the truth. One issue that has not been discussed is the role that the CICE perturbed parameters could play in snow evolution. Perturbed parameters have been used over the years to create more spread in atmospheric models (Murphy et al., 2004; Stainforth et al., 2005; Christensen et al., 2015; Orth et al., 2016), where the system is more chaotic. However, the impact the perturbed parameters would have on a less-chaotic system such as the cryosphere is unclear. Concerning total snow volume, there are larger and more significant correlations between the R_{snow} parameter compared with the other perturbed parameters throughout the cycling period (Fig. 12A). The positive correlations indicate that larger standard deviations of the dry snow grain radius lead to greater total snow volume. This connection is a result of the larger standard deviations of dry snow grain radius resulting in a higher albedo, reflecting more incoming shortwave radiation (Hunke et al., 2015). Looking at snow melt, there are negative and significant correlations during the melt season for the R_{snow} parameter, while the other parameters have little significant correlations (Fig. 12B). This means there is more snow melt for lower standard deviations of dry snow grain radius, resulting in more absorbed shortwave radiation due to a lower surface albedo. The R_{snow} parameter for the truth member is located above the 75th percentile compared with the rest of the perturbed R_{snow} parameters (Fig. 12C). Even with snow assimilation updates, the impact of the perturbed R_{snow} parameter might play a larger role in snow evolution. Due to this fact, it is not surprising to find that the ensemble mean is negatively biased compared to the truth for total snow volume.

4 Conclusions

To advance our understanding of the global climate, it is critical to improve our representation of the different underlying Earth-system components within our coupled numerical climate models. One important Earth-system component—the cryosphere—has gathered recent attention due to declining Arctic summer sea ice and its link back to Arctic amplification. Data assimilation methods, such as the ensemble Kalman filter (EnKF), are one way to improve the representation of sea ice states by exploiting information from observations taken from satellites. However, the formulation of the EnKF has Gaussian assumptions and most state variables representing sea ice have some form of boundedness, which can lead to non-Gaussian distributions near those bounds. This study investigates the data assimilation impacts of the non-Gaussian nature of sea ice and snow variables on the generation of analyses within different observing system simulation experiments (OSSEs). The different OSSEs presented in this study will investigate which data assimilation setup provides the most accurate representation of sea ice and snow when dealing with non-Gaussian observations and state variables.

In this study, a sea ice model called CICE is coupled to the ensemble data assimilation software provided by DART to obtain a sea ice modeling system called CICE-DART. CICE-DART is used to conduct OSSEs to test different data assimilation configurations and the assimilation of different sea ice and snow observation subsets synthetically generated from a truth member. Six different experiments were completed to test different observation combinations, data assimilation techniques, and post-processing updates (Table 1).

The first three experiments explore the impact of different assimilated synthetic observation subsets on the generation of the most accurate forecasts for both sea ice and snow states. According to the daily biases and aggregated statistics, EAKF-ThickSnow is more accurate, when compared to the truth, for sea ice area, sea ice volume, and snow volume. This highlights the negative impacts that SIC observations have on forecasts when they are assimilated in EAKF-ConcThick and EAKF-ConcThickSnow. This result contradicts previous studies that found positive impacts from assimilating SIC observations (Sakov et al., 2012a; Massonnet et al., 2015; Posey et al., 2015). However, this result could be linked to differences in the observation error specification chosen for SIC observations in the different studies. In our study, early springtime SIC truth values are still close to one, maximizing their observation error (15% of the truth value), which leads to synthetic SIC observations being drawn further below the truth due to the bound at one. In addition, the prior spread increases because of the onset of springtime melt and prior inflation. Combining the low-bias observations with the increase in the prior spread leads to an enhancement of the non-Gaussian effects during early springtime. A similar but opposite effect (high-biased SIC observations) would be observed during winter; however, prior ensemble spread in the modeled SIC fields is smaller, resulting in a lower weighting of SIC observations. While potentially different from other studies, our chosen SIC observation error specification intensified the non-Gaussian effects of assimilating SIC observations while also showing the potential impact accurate SIC observations can have during data assimilation multivariate updating. Interestingly, SIC observations do provide positive updates in the marginal ice zone, as shown by SPS and total IIEE being lower in EAKF-ConcThick and EAKF-ConcThickSnow. Because of positive updates in the marginal ice zone, it would be optimal to assimilate SIC observations within the data assimilation system.

Additional OSSEs are performed to further investigate potential data assimilation improvements for sea ice (Table 1). A non-Gaussian RHF was tested since it was developed for non-Gaussian situations. The results showed little improvement over the EAKF when assimilating SIC observations. This is likely linked back to the RHF making some non-Gaussian assumptions on the tails and assumed normal likelihood when the distribution is not bounded. The modification to the forward operators did not improve sea ice data assimilation, especially regarding sea ice edge errors. This could mean that there are few instances of shuffling the sea ice thickness distribution due to prior inflation. Additionally, the multivariate update between sea ice thickness observations and sea ice area might be the reason for the increase in sea ice edge errors. Lastly, assimilating SISTs did not lead to increased skill for sea ice variables. The correction between the SISTs and sea ice model variables might not be significant, leading to little improvement.

To better understand the assimilation impacts due to the SIC observations, a simplified data assimilation experiment is completed. This simplified experiment mimics central Arctic SIC during the winter time, meaning the truth does not change. Regardless of the filter type or observation error value, the prior ensemble mean moves away from the truth and closer to the average observation value during the cycling period. These experiments verified that near a bound, the performance of the EAKF and the RHF is suboptimal. We believe the suboptimal performance is linked back to using a truncated normal distribution as the observation error distribution while the observation likelihood for the EAKF and RHF is assumed to be normal. Future projects focusing on sea ice data assimilation might want to consider a different choice for the observation likelihood specification, similar to those laid out in Anderson (2022). This would include using distributions for the prior PDF

and the observation likelihood that are similar to the observation error distribution and consider the bounds more appropriately
485 (e.g., a truncated Gaussian distribution).

The evaluation of the additional OSSEs is performed to investigate their impact on snow updates. The improvements associ-
ated with using the non-Gaussian RHF over the EAKF were small for snow volume. This means that the non-Gaussian impacts
from the SIC observations were negative for snow volume updates. Additionally, the modified forward operators have little
impact on snow volume updates. However, there is a slight improvement in the snow volume when SISTs are assimilated. This
490 improvement occurred during May and not over a specific area of sea ice. This could mean that the connections between SISTs
and snow are more significant than those between sea ice, where the impacts were less impactful. Regardless, all additional
experiments still experienced a negative bias throughout the entire cycling period. Further investigation revealed that one of
the perturbed parameters could be driving the negative bias for snow volume. Correlations were larger and significant between
snow variables and the representation of the dry snow grain radius size (R_{snow}) within our ensemble. Due to the random choice
495 of the R_{snow} parameter for the truth member, it is likely that the ensemble mean is negatively biased for snow volume.

Future work will further investigate how to properly assimilate SIC observations. Because of their positive impact on the
marginal ice zone, an experiment could be proposed in which only SIC observations are assimilated in that remote location.
Additionally, further investigation is needed to test the use of more sophisticated data assimilation methods that accurately
handle non-Gaussian distributions. The RHF can represent non-Gaussian priors and arbitrary likelihoods for the observed
500 variables. The RHF can be modified to work with bounded quantities (Anderson, 2020, 2022), which should be investigated in
future studies. Lastly, supplementary OSSE experiments could be completed with a different ensemble member chosen as the
truth to further understand the impacts of the perturbed parameters on representing snow volume. These additional experiments
will further help us understand the correct data assimilation setup for representing sea ice and snow in climate analyses.

Code availability. CICE version 5 used for the experiments described here is part of the CESM2 framework which is publicly available for
505 download from <https://www.cesm.ucar.edu/models/cesm2/download.html> (accessed in August of 2020). The data assimilation software used
here can be downloaded from <https://github.com/NCAR/DART> (accessed in August of 2020).

Data availability. The perturbed CICE parameters used in this study is publicly available for download from <https://doi.org/10.5281/zenodo.8164431>.
Post-processed and raw data from the experiments described here are stored on NCAR's campaign storage.

Author contributions. The development of the CICE-DART framework was completed by both CR and JA. CR prepared and performed the
510 experiments under the supervision of JA. The manuscript was composed by CR with contributions and feedback from JA.

Competing interests. The contact author has declared that neither they nor their co-author have any competing interests.

Acknowledgements. This material is based upon work supported by the National Center for Atmospheric Research, which is a major facility sponsored by the National Science Foundation under Cooperative Agreement No. 1755088. Special thanks to the entire DART team for providing helpful input and source code support. I would also like to thank Cecilia Bitz and Molly Wieringa for their fruitful discussions. We
515 thank the editor and anonymous reviewers for constructive comments that helped improve the manuscript.

References

- Anderson, J., Hoar, T., Raeder, K., Liu, H., Collins, N., Torn, R., and Avellano, A.: The Data Assimilation Research Testbed: A community facility, *Bull. Amer. Meteor. Soc.*, 90, 1283–1296, 2009.
- Anderson, J. L.: An Ensemble Adjustment Kalman Filter for Data Assimilation, *Mon. Wea. Rev.*, 129, 2884–2903, 2001.
- 520 Anderson, J. L.: An adaptive covariance inflation error correction algorithm for ensemble filters, *Tellus*, 59A, 210–224, 2007.
- Anderson, J. L.: A non-Gaussian ensemble filter update for data assimilation, *Mon. Wea. Rev.*, 138, 4186–4198, 2010.
- Anderson, J. L.: A marginal adjustment rank histogram filter for non-Gaussian ensemble data assimilation, *Mon. Wea. Rev.*, 148, 3361–3378, 2020.
- Anderson, J. L.: A Quantile-Conserving Ensemble Filter Framework. Part I: Updating an Observed Variable, *Mon. Wea. Rev.*, 150, 1061–
525 1074, 2022.
- Barth, A., Canter, M., Van Schaeybroeck, B., Vannitsem, S., Massonnet, F., Zunz, V., Mathiot, P., Alvera-Azcarate, A., and Beckers, J.-M.: Assimilation of sea surface temperature, sea ice concentration and sea ice drift in a model of the Southern Ocean, *Ocn. Modelling*, 93, 22–39, 2015.
- Briegleb, B. and Light, B.: A delta-Eddington multiple scattering parameterization for solar radiation in the sea ice component of the 625
530 Community Climate System Model, Tech. rep., NCAR Technical Note NCAR/TN-472+ STR, <https://doi.org/10.5065/D6B27S71>, 2007.
- Burgers, G., Van Leeuwen, P. J., and Evensen, G.: Analysis scheme in the ensemble Kalman filter, *Mon. Wea. Rev.*, 126, 1719–1724, 1998.
- Chen, Z., Liu, J., Song, M., Yang, Q., and Xu, S.: Impacts of assimilating satellite sea ice concentration and thickness on Arctic sea ice prediction in the NCEP Climate Forecast System, *J. Climate*, 30, 8429–8446, 2017.
- Cheng, S., Chen, Y., Aydoğdu, A., Bertino, L., Carrassi, A., Rampal, P., and Jones, C. K.: Arctic sea ice data assimilation combining an
535 ensemble Kalman filter with a novel Lagrangian sea ice model for the winter 2019–2020, *The Cryosphere*, 17, 1735–1754, 2023.
- Christensen, H., Moroz, I., and Palmer, T.: Simulating weather regimes: Impact of stochastic and perturbed parameter schemes in a simple atmospheric model, *Climate Dyn.*, 44, 2195–2214, 2015.
- Chung, E.-S., Ha, K.-J., Timmermann, A., Stuecker, M. F., Bodai, T., and Lee, S.-K.: Cold-season Arctic amplification driven by Arctic ocean-mediated seasonal energy transfer, *Earth’s Future*, 9, e2020EF001 898, 2021.
- 540 Danabasoglu, G., Lamarque, J.-F., Bacmeister, J., Bailey, D., DuVivier, A., Edwards, J., Emmons, L., Fasullo, J., Garcia, R., Gettelman, A., et al.: The community earth system model version 2 (CESM2), *J. Adv. Mod. Ear. Sys.*, 12, e2019MS001 916, 2020.
- Day, J., Hawkins, E., and Tietsche, S.: Will Arctic sea ice thickness initialization improve seasonal forecast skill?, *Geophys. Res. Lett.*, 41, 7566–7575, 2014.
- Dirkson, A., Merryfield, W. J., and Monahan, A.: Impacts of sea ice thickness initialization on seasonal Arctic sea ice predictions, *J. Climate*,
545 30, 1001–1017, 2017.
- England, M. R., Eisenman, I., Lutsko, N. J., and Wagner, T. J.: The recent emergence of Arctic Amplification, *Geophys. Res. Lett.*, 48, e2021GL094 086, 2021.
- Evensen, G.: The ensemble Kalman filter: Theoretical formulation and practical implementation, *Ocean dyn.*, 53, 343–367, 2003.
- Fiedler, E. K., Martin, M. J., Blockley, E., Mignac, D., Fournier, N., Ridout, A., Shepherd, A., and Tilling, R.: Assimilation of sea ice
550 thickness derived from CryoSat-2 along-track freeboard measurements into the Met Office’s Forecast Ocean Assimilation Model (FOAM), *Cryosphere*, 16, 61–85, 2022.

- Fowler, A. and Jan Van Leeuwen, P.: Observation impact in data assimilation: the effect of non-Gaussian observation error, *Tellus A: Dyn. Meteor. Ocn.*, 65, 20035, 2013.
- 555 Fritzner, S., Graversen, R., Christensen, K. H., Rostovsky, P., and Wang, K.: Impact of assimilating sea ice concentration, sea ice thickness and snow depth in a coupled ocean–sea ice modelling system, *The Cryosphere*, 13, 491–509, 2019.
- Fritzner, S. M., Graversen, R. G., Wang, K., and Christensen, K. H.: Comparison between a multi-variate nudging method and the ensemble Kalman filter for sea-ice data assimilation, *Journal of Glaciology*, 64, 387–396, 2018.
- Gaspari, G. and Cohn, S. E.: Construction of correlation functions in two and three dimensions, *Quart. J. Roy. Meteor. Soc.*, 125, 723–757, 1999.
- 560 Goessling, H. and Jung, T.: A probabilistic verification score for contours: Methodology and application to Arctic ice-edge forecasts, *Quart. J. Roy. Meteor. Soc.*, 144, 735–743, 2018.
- Goessling, H. F., Tietsche, S., Day, J. J., Hawkins, E., and Jung, T.: Predictability of the Arctic sea ice edge, *Geophys. Res. Lett.*, 43, 1642–1650, 2016.
- 565 Hall, D. K., Nghiem, S. V., Rigor, I. G., and Miller, J. A.: Uncertainties of temperature measurements on snow-covered land and sea ice from in situ and MODIS data during BROMEX, *J. Climate Appl. Meteor.*, 54, 966–978, 2015.
- Holland, M. M. and Bitz, C. M.: Polar amplification of climate change in coupled models, *Climate Dyn.*, 21, 221–232, 2003.
- Holland, M. M., Clemens-Sewall, D., Landrum, L., Light, B., Perovich, D., Polashenski, C., Smith, M., and Webster, M.: The influence of snow on sea ice as assessed from simulations of CESM2, *Cryosphere*, 15, 4981–4998, 2021.
- Houtekamer, P. L. and Zhang, F.: Review of the ensemble Kalman filter for atmospheric data assimilation, *Mon. Wea. Rev.*, 144, 4489–4532, 570 2016.
- Hunke, E. C., Lipscomb, W. H., Turner, A. K., Jeffery, N., and Elliott, S.: CICE: The Los Alamos Sea Ice Model documentation and software user’s manual, version 5.1, Los Alamos National Laboratory Doc., LA-CC-06-012, 116, 2015.
- Jansen, E., Christensen, J. H., Dokken, T., Nisancioglu, K. H., Vinther, B. M., Capron, E., Guo, C., Jensen, M. F., Langen, P. L., Pedersen, R. A., et al.: Past perspectives on the present era of abrupt Arctic climate change, *Nat. Clim. Change*, 10, 714–721, 2020.
- 575 Jenkins, M. and Dai, A.: The Impact of Sea-Ice Loss on Arctic Climate Feedbacks and Their Role for Arctic Amplification, *Geophys. Res. Lett.*, 48, e2021GL094 599, 2021.
- Kalman, R. E.: A new approach to linear filtering and prediction problems, *Trans. ASME*, 82, 35–45, 1960.
- Kimmritz, M., Counillon, F., Bitz, C., Massonnet, F., Bethke, I., and Gao, Y.: Optimising assimilation of sea ice concentration in an Earth system model with a multicategory sea ice model, *Tellus: Dyn. Meteor. Ocn.*, 70, 1–23, 2018.
- 580 Kwok, R. and Cunningham, G.: ICESat over Arctic sea ice: Estimation of snow depth and ice thickness, *J. Geophys. Res.: Oceans*, 113, 2008.
- Lawson, W. G. and Hansen, J. A.: Implications of stochastic and deterministic filters as ensemble-based data assimilation methods in varying regimes of error growth, *Mon. Wea. Rev.*, 132, 1966–1981, 2004.
- Lei, J., Bickel, P., and Snyder, C.: Comparison of ensemble Kalman filters under non-Gaussianity, *Mon. Wea. Rev.*, 138, 1293–1306, 2010.
- 585 Lindsay, R. and Zhang, J.: Assimilation of ice concentration in an ice–ocean model, *J. Atmos. Oceanic Technol.*, 23, 742–749, 2006.
- Lipscomb, W. H.: Remapping the thickness distribution in sea ice models, *J. Geophys. Res. Oceans*, 106, 13 989–14 000, 2001.
- Lisæter, K. A., Rosanova, J., and Evensen, G.: Assimilation of ice concentration in a coupled ice–ocean model, using the Ensemble Kalman filter, *Ocn. Dyn.*, 53, 368–388, 2003.
- Lu, P., Li, Z., Cheng, B., and Leppäranta, M.: A parameterization of the ice-ocean drag coefficient, *J. Geophys. Res. Oceans*, 116, 2011.

- 590 Maaß, N., Kaleschke, L., Tian-Kunze, X., and Drusch, M.: Snow thickness retrieval over thick Arctic sea ice using SMOS satellite data, *The Cryosphere*, 7, 1971–1989, 2013.
- Massonnet, F., Fichefet, T., and Goosse, H.: Prospects for improved seasonal Arctic sea ice predictions from multivariate data assimilation, *Ocean Modelling*, 88, 16–25, 2015.
- Mathiot, P., König Beatty, C., Fichefet, T., Goosse, H., Massonnet, F., and Vancoppenolle, M.: Better constraints on the sea-ice state using
595 global sea-ice data assimilation, *Geoscientific Model Development*, 5, 1501–1515, 2012.
- Meier, W. N. and Maslanik, J. A.: Effect of environmental conditions on observed, modeled, and assimilated sea ice motion errors, *J. Geophys. Res.: Oceans*, 108, 2003.
- Meier, W. N., Fetterer, F., Windnagel, A. K., and Stewart, J. S.: NOAA/NSIDC Climate Data Record of Passive Microwave Sea Ice Concentration, Version 4, <https://doi.org/10.7265/efmz-2t65>, 2021.
- 600 Metref, S., Cosme, E., Snyder, C., and Brasseur, P.: A non-Gaussian analysis scheme using rank histograms for ensemble data assimilation, *Nonlinear Processes Geophys.*, 21, 869–885, 2014.
- Msadek, R., Vecchi, G. A., Winton, M., and Gudgel, R. G.: Importance of initial conditions in seasonal predictions of Arctic sea ice extent, *Geophys. Res. Lett.*, 41, 5208–5215, 2014.
- Mu, L., Yang, Q., Losch, M., Losa, S. N., Ricker, R., Nerger, L., and Liang, X.: Improving sea ice thickness estimates by assimilating
605 CryoSat-2 and SMOS sea ice thickness data simultaneously, *Quart. J. Roy. Meteor. Soc.*, 144, 529–538, 2018.
- Murphy, J., Sexton, D., Barnett, D., Jones, G., Webb, M., Collins, M., and Stainforth, D.: Quantifying uncertainties in climate change from a large ensemble of general circulation model predictions, *Nature*, 430, 768–772, 2004.
- Orth, R., Dutra, E., and Pappenberger, F.: Improving weather predictability by including land surface model parameter uncertainty, *Mon. Wea. Rev.*, 144, 1551–1569, 2016.
- 610 Pham, D. T.: Stochastic methods for sequential data assimilation in strongly nonlinear systems, *Mon. Wea. Rev.*, 129, 1194–1207, 2001.
- Pires, C. A., Talagrand, O., and Bocquet, M.: Diagnosis and impacts of non-Gaussianity of innovations in data assimilation, *Physica D: Nonlin. Phenom.*, 239, 1701–1717, 2010.
- Posey, P. G., Metzger, E., Wallcraft, A., Hebert, D., Allard, R., Smedstad, O., Phelps, M., Fetterer, F., Stewart, J., Meier, W., et al.: Improving Arctic sea ice edge forecasts by assimilating high horizontal resolution sea ice concentration data into the US Navy’s ice forecast systems,
615 *The Cryosphere*, 9, 1735–1745, 2015.
- Raeder, K., Hoar, T. J., El Gharamti, M., Johnson, B. K., Collins, N., Anderson, J. L., Stewart, J., and Coady, M.: A new CAM6+DART reanalysis with surface forcing from CAM6 to other CESM models, *Scientific Reports*, 11, 1–24, 2021.
- Rantanen, M., Karpechko, A. Y., Lipponen, A., Nordling, K., Hyvärinen, O., Ruosteenoja, K., Vihma, T., and Laaksonen, A.: The Arctic has warmed nearly four times faster than the globe since 1979, *Communications Earth & Environment*, 3, 1–10, 2022.
- 620 Ricker, R., Hendricks, S., Kaleschke, L., Tian-Kunze, X., King, J., and Haas, C.: A weekly Arctic sea-ice thickness data record from merged CryoSat-2 and SMOS satellite data, *Cryosphere*, 11, 1607–1623, 2017.
- Rostosky, P., Spreen, G., Farrell, S. L., Frost, T., Heygster, G., and Melsheimer, C.: Snow depth retrieval on Arctic sea ice from passive microwave radiometers—Improvements and extensions to multiyear ice using lower frequencies, *Journal of Geophysical Research: Oceans*, 123, 7120–7138, 2018.
- 625 Rostosky, P., Spreen, G., Gerland, S., Huntemann, M., and Mech, M.: Modeling the microwave emission of snow on Arctic sea ice for estimating the uncertainty of satellite retrievals, *J. Geophys. Res. Oceans*, 125, e2019JC015465, 2020.

- Sakov, P., Counillon, F., Bertino, L., Lisæter, K., Oke, P., and Korablev, A.: TOPAZ4: an ocean-sea ice data assimilation system for the North Atlantic and Arctic, *Ocn. Science*, 8, 633–656, 2012a.
- Sakov, P., Oliver, D. S., and Bertino, L.: An iterative EnKF for strongly nonlinear systems, *Mon. Wea. Rev.*, 140, 1988–2004, 2012b.
- 630 Screen, J. A. and Simmonds, I.: The central role of diminishing sea ice in recent Arctic temperature amplification, *Nature*, 464, 1334–1337, 2010.
- Serreze, M., Barrett, A., Stroeve, J., Kindig, D., and Holland, M.: The emergence of surface-based Arctic amplification, *Cryosphere*, 3, 11–19, 2009.
- Serreze, M. C. and Francis, J. A.: The Arctic amplification debate, *Climate Change*, 76, 241–264, 2006.
- 635 Stainforth, D. A., Aina, T., Christensen, C., Collins, M., Faull, N., Frame, D. J., Kettleborough, J. A., Knight, S., Martin, A., Murphy, J., et al.: Uncertainty in predictions of the climate response to rising levels of greenhouse gases, *Nature*, 433, 403–406, 2005.
- Stark, J. D., Ridley, J., Martin, M., and Hines, A.: Sea ice concentration and motion assimilation in a sea ice- ocean model, *J. Geophys. Res.: Oceans*, 113, 2008.
- Sturm, M. and Massom, R. A.: Snow in the sea ice system: friend or foe?, *Sea ice*, pp. 65–109, 2017.
- 640 Tietsche, S., Day, J. J., Guemas, V., Hurlin, W., Keeley, S., Matei, D., Msadek, R., Collins, M., and Hawkins, E.: Seasonal to interannual Arctic sea ice predictability in current global climate models, *Geophys. Res. Lett.*, 41, 1035–1043, 2014.
- Tilling, R. L., Ridout, A., and Shepherd, A.: Near-real-time Arctic sea ice thickness and volume from CryoSat-2, *Cryosphere*, 10, 2003–2012, 2016.
- Tippett, M. K., Anderson, J. L., Bishop, C. H., Hamill, T. M., and Whitaker, J. S.: Ensemble Square Root Filters, *Mon. Wea. Rev.*, 131, 2003.
- 645 Urrego-Blanco, J. R., Urban, N. M., Hunke, E. C., Turner, A. K., and Jeffery, N.: Uncertainty quantification and global sensitivity analysis of the Los Alamos sea ice model, *J. Geophys. Res. Oceans*, 121, 2709–2732, 2016.
- Van Woert, M. L., Zou, C.-Z., Meier, W. N., Hovey, P. D., Preller, R. H., and Posey, P. G.: Forecast verification of the Polar Ice Prediction System (PIPS) sea ice concentration fields, *Journal Atmos. Ocn. Tech.*, 21, 944–957, 2004.
- Walsh, J. E.: Intensified warming of the Arctic: Causes and impacts on middle latitudes, *Glob. Planet. Change*, 117, 52–63, 2014.
- 650 Welch, B. L.: The generalization of ‘STUDENT’S’ problem when several different population variances are involved, *Biometrika*, 34, 28–35, 1947.
- Xie, J., Counillon, F., Bertino, L., Tian-Kunze, X., and Kaleschke, L.: Benefits of assimilating thin sea ice thickness from SMOS into the TOPAZ system, *The Cryosphere*, 10, 2745–2761, 2016.
- Xie, J., Counillon, F., and Bertino, L.: Impact of assimilating a merged sea-ice thickness from CryoSat-2 and SMOS in the Arctic reanalysis, *The Cryosphere*, 12, 3671–3691, 2018.
- 655 Yu, L., Zhong, S., Vihma, T., and Sun, B.: Attribution of late summer early autumn Arctic sea ice decline in recent decades, *npj Clim. and Atmos. Sci.*, 4, 1–14, 2021.
- Zampieri, L., Goessling, H. F., and Jung, T.: Bright prospects for Arctic sea ice prediction on subseasonal time scales, *Geophys. Res. Lett.*, 45, 9731–9738, 2018.
- 660 Zhang, Y.-F., Bitz, C. M., Anderson, J. L., Collins, N., Hendricks, J., Hoar, T., Raeder, K., and Massonnet, F.: Insights on sea ice data assimilation from perfect model observing system simulation experiments, *J. Climate*, 31, 5911–5926, 2018.
- Zygmuntowska, M., Rampal, P., Ivanova, N., and Smedsrud, L. H.: Uncertainties in Arctic sea ice thickness and volume: new estimates and implications for trends, *The Cryosphere*, 8, 705–720, 2014.

Table 1. List of CICE-DART OSSEs with the different configurations.

Experiments	Assimilated Observations	Modified Forward Operator	Postprocessed States	Assimilation Algorithm	Data Assimilation Updated State Vector
EAKF-ConcThick	SIC SIT	No	Category Snow Volume	EAKF	Category Sea Ice Area Category Sea Ice Volume
EAKF-ConcThickSnow	SIC SIT D_{snow}	No	No	EAKF	Category Sea Ice Area Category Sea Ice Volume Category Snow Volume
EAKF-ThickSnow	SIT D_{snow}	No	No	EAKF	Category Sea Ice Area Category Sea Ice Volume Category Snow Volume
RHF-ConcThickSnow	SIC SIT D_{snow}	No	No	RHF	Category Sea Ice Area Category Sea Ice Volume Category Snow Volume
EAKF-ModifiedFO	SIT D_{snow}	Yes	No	EAKF	Category Sea Ice Area Category Sea Ice Volume Category Snow Volume
EAKF-SIST	SIT D_{snow} SIST	No	No	EAKF	Category Sea Ice Area Category Sea Ice Volume Category Snow Volume

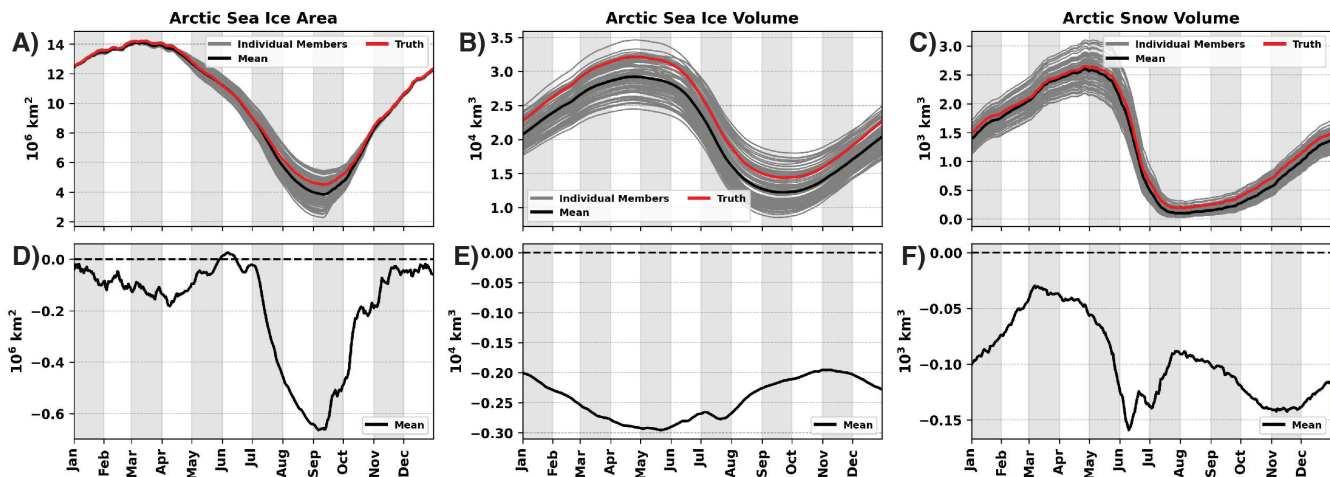


Figure 1. Daily total Arctic (A) sea ice area, (B) sea ice volume, and (C) snow volume from CICE5 free forecast simulations. Each gray line represents an individual ensemble member, black line represents the ensemble mean, and the red line represents the truth member. The truth member is a randomly selected ensemble member. Daily biases of the total Arctic (A) sea ice area, (B) sea ice volume, and (C) snow volume where the black line represents the ensemble mean difference compared to the truth. The black dashed line is the zero reference line. The free forecast period is for the year 2013.

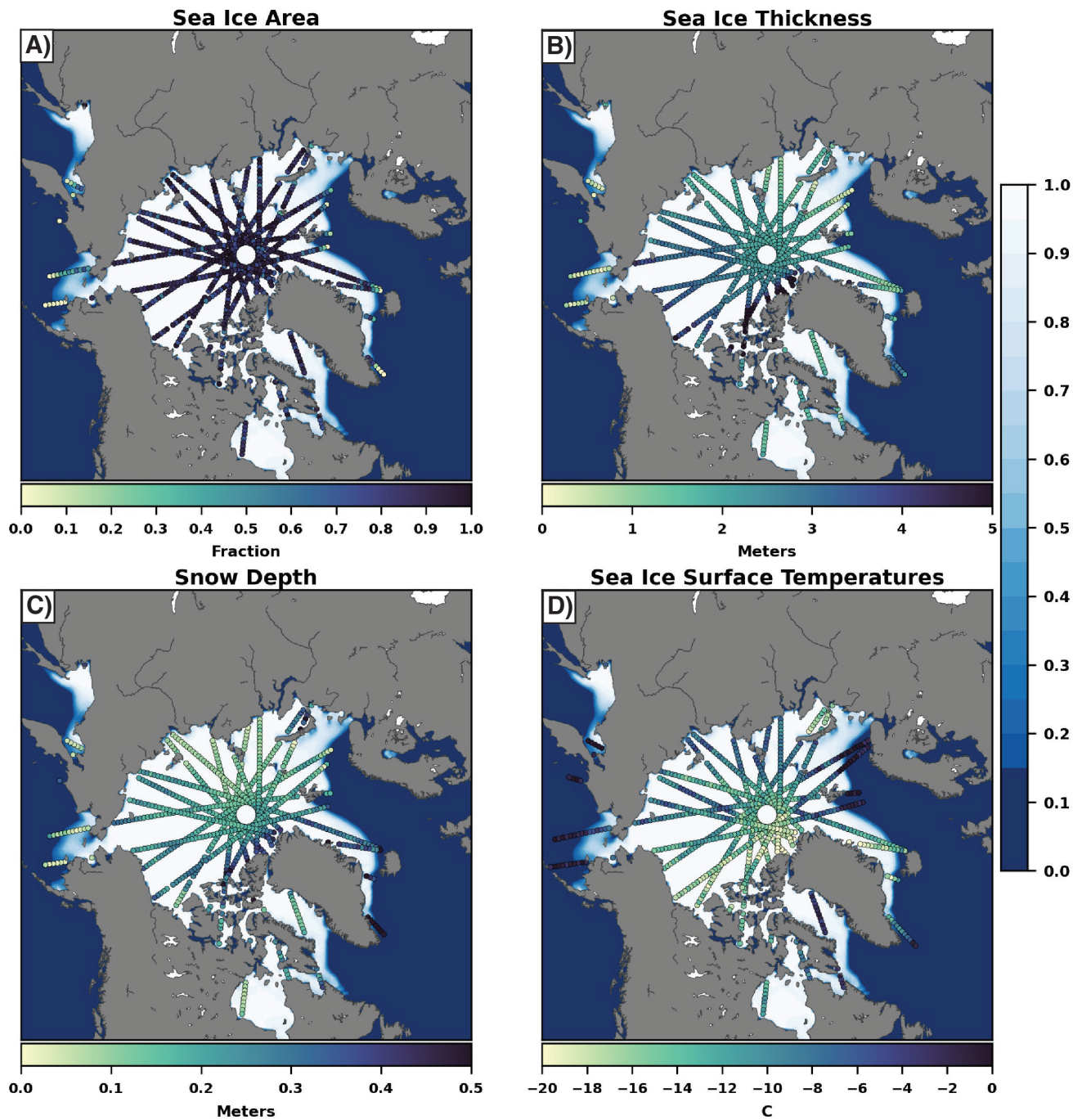


Figure 2. A snapshot example of the spatial locations of the OSSE synthetically generated (A) sea ice area, (B) sea ice thickness, (C) snow depth and (D) sea ice surface temperature observations that are assimilated. The observation locations are from Cryosat-2 latitude and longitude ground tracks. Colorfill is the ensemble mean of the sea ice area and the dots are the observation locations along with their associated value.

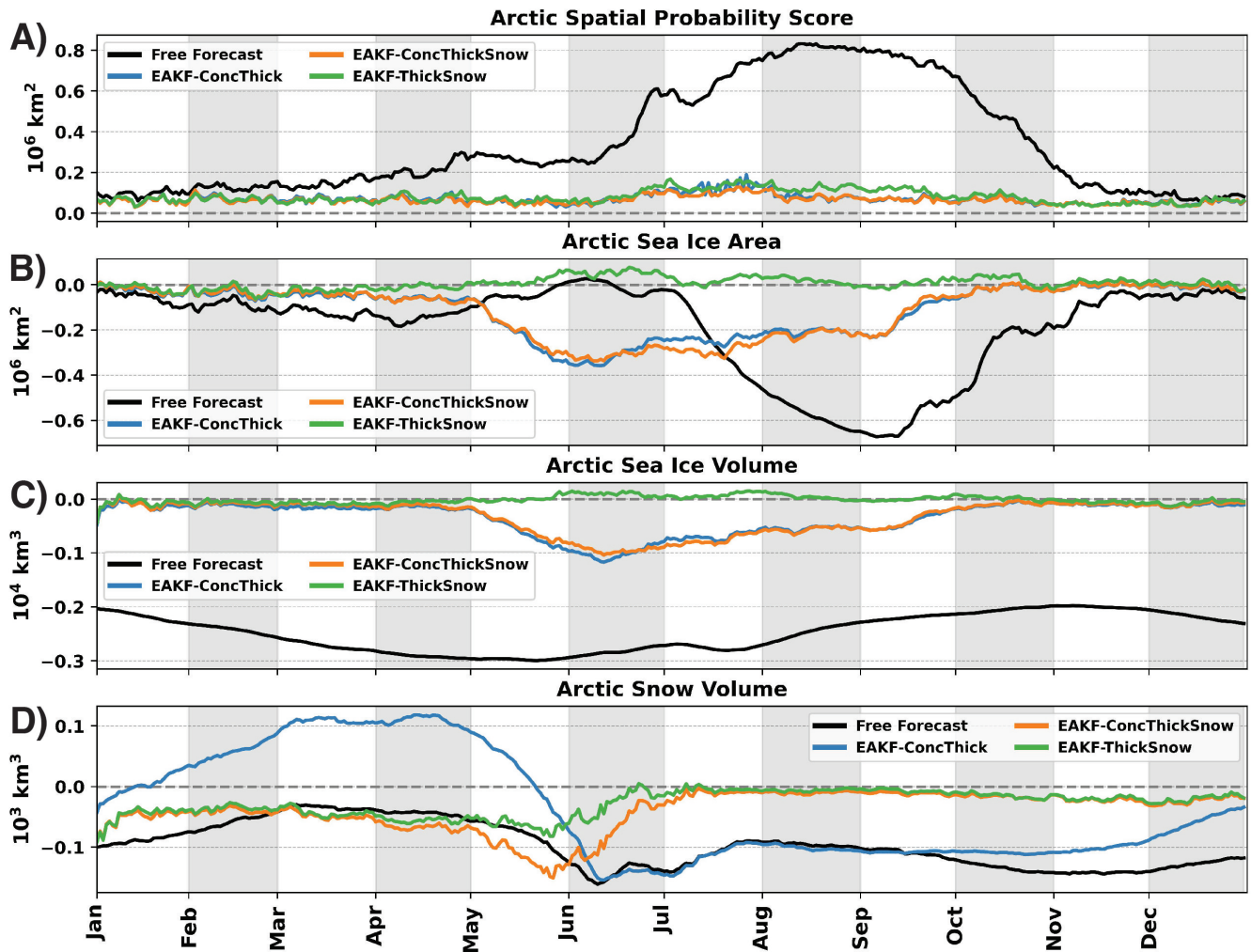


Figure 3. (A) Daily Arctic spatial probability score for the free forecasts, EAKF-ConcThick, EAKF-ConcThickSnow, and EAKF-ThickSnow. Daily biases of the Arctic total (B) sea ice area, (C) sea ice volume, and (D) snow volume from the free forecasts, EAKF-ConcThick, EAKF-ConcThickSnow, and EAKF-ThickSnow. Gray dashed lines are the zero reference line.

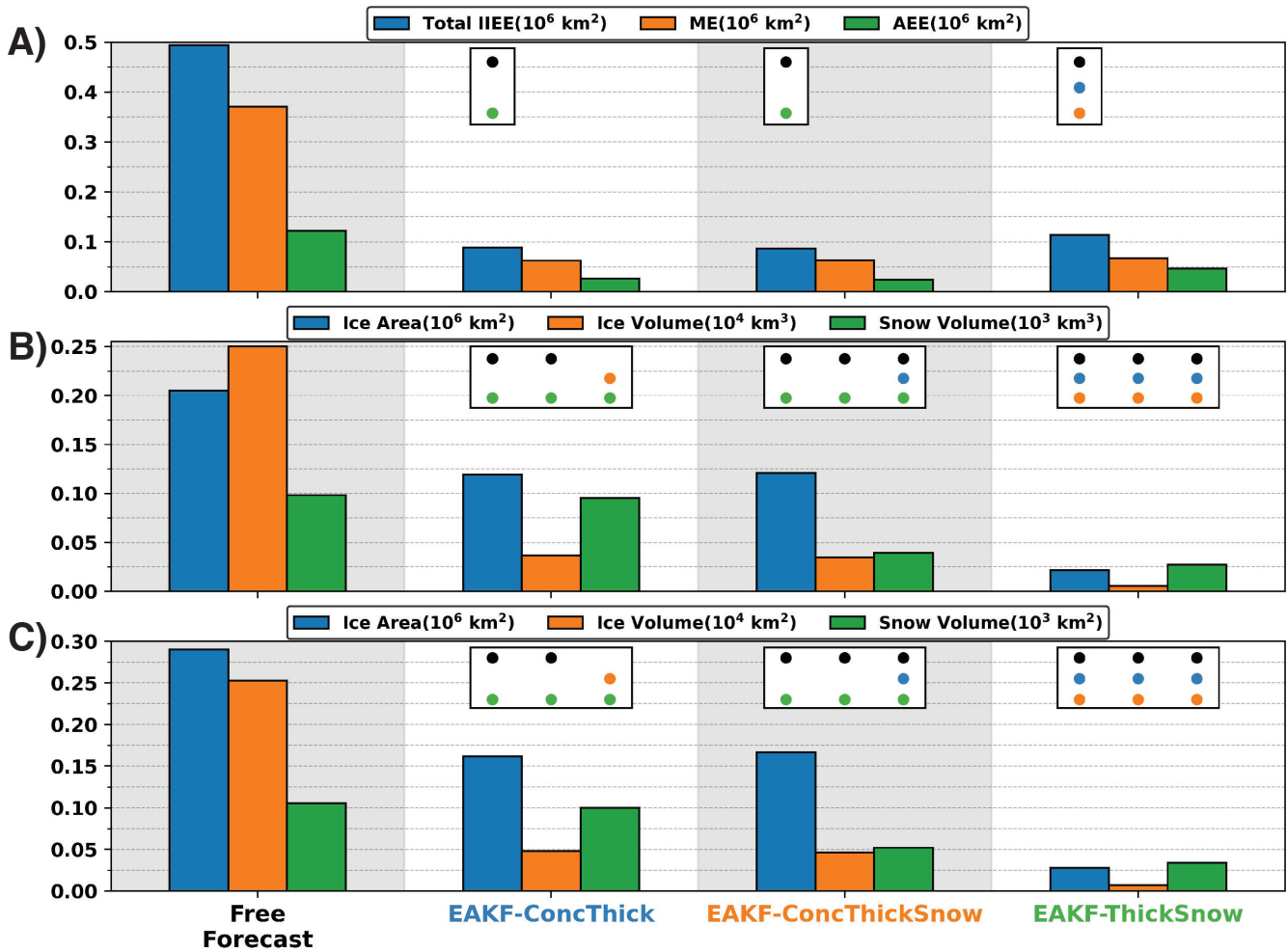


Figure 4. The (A) IIEE, (B) MAB, and (C) RMSE of sea ice area, sea ice volume and snow volume from the free forecast, EAKF-ConcThick, EAKF-ConcThickSnow, and EAKF-ThickSnow. Each index is computed using the ensemble mean and over the entire cycling period. Dots represents any pairs of experiments that are significantly different from a different experiment using a student t-test. Dot colors correspond to the different experiments.

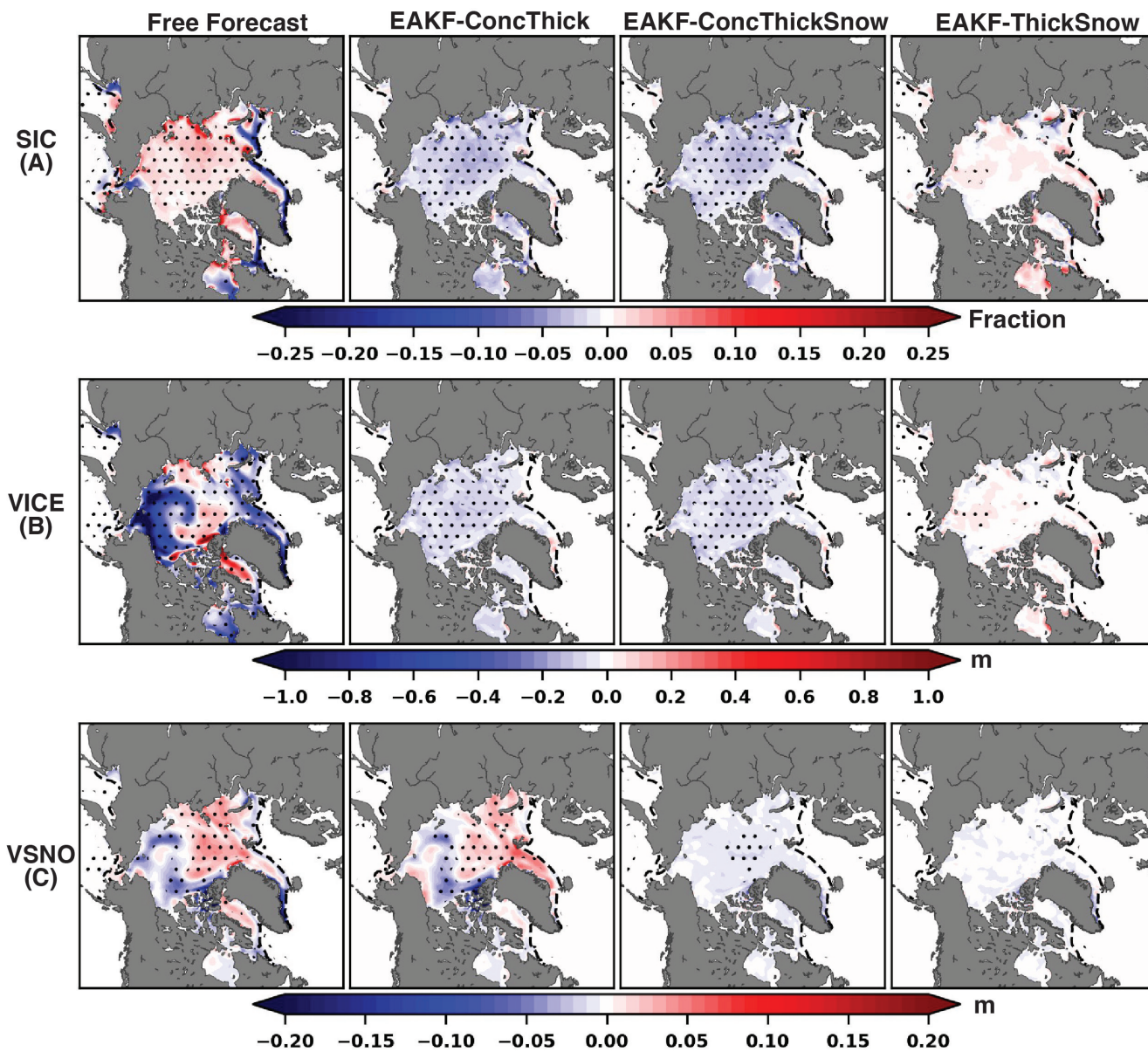


Figure 5. Ensemble mean spatial biases of (A) SIC, (B) V_{ice} , and (C) V_{snow} averaged over May–June for the free forecast, EAKF-ConcThick, EAKF-ConcThickSnow, and EAKF-ThickSnow. Stippling represents significant biases at the 95% confidence interval using a Welch's t-test. The black dashed line is the sea ice edge (0.15 SIC).

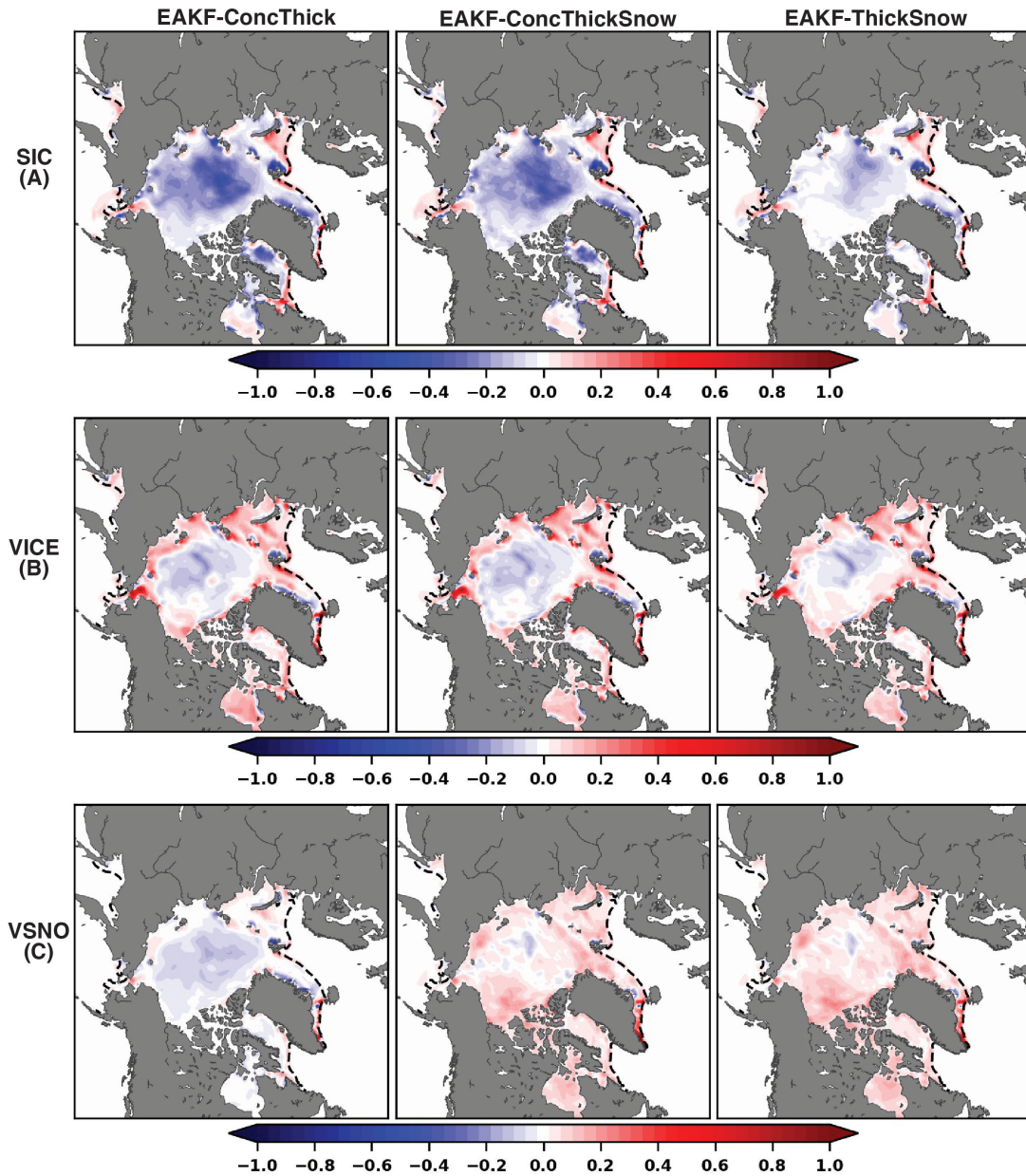


Figure 6. Normalized spatial analysis increments of (A) SIC, (B) V_{ice} , and (C) V_{snow} averaged over May–June for EAKF-ConcThick, EAKF-ConcThickSnow, and EAKF-ThickSnow. Analysis increments of SIC, V_{ice} , and V_{snow} were normalized using the largest absolute value from across the three experiments. The black dashed line is the sea ice edge (0.15 SIC).

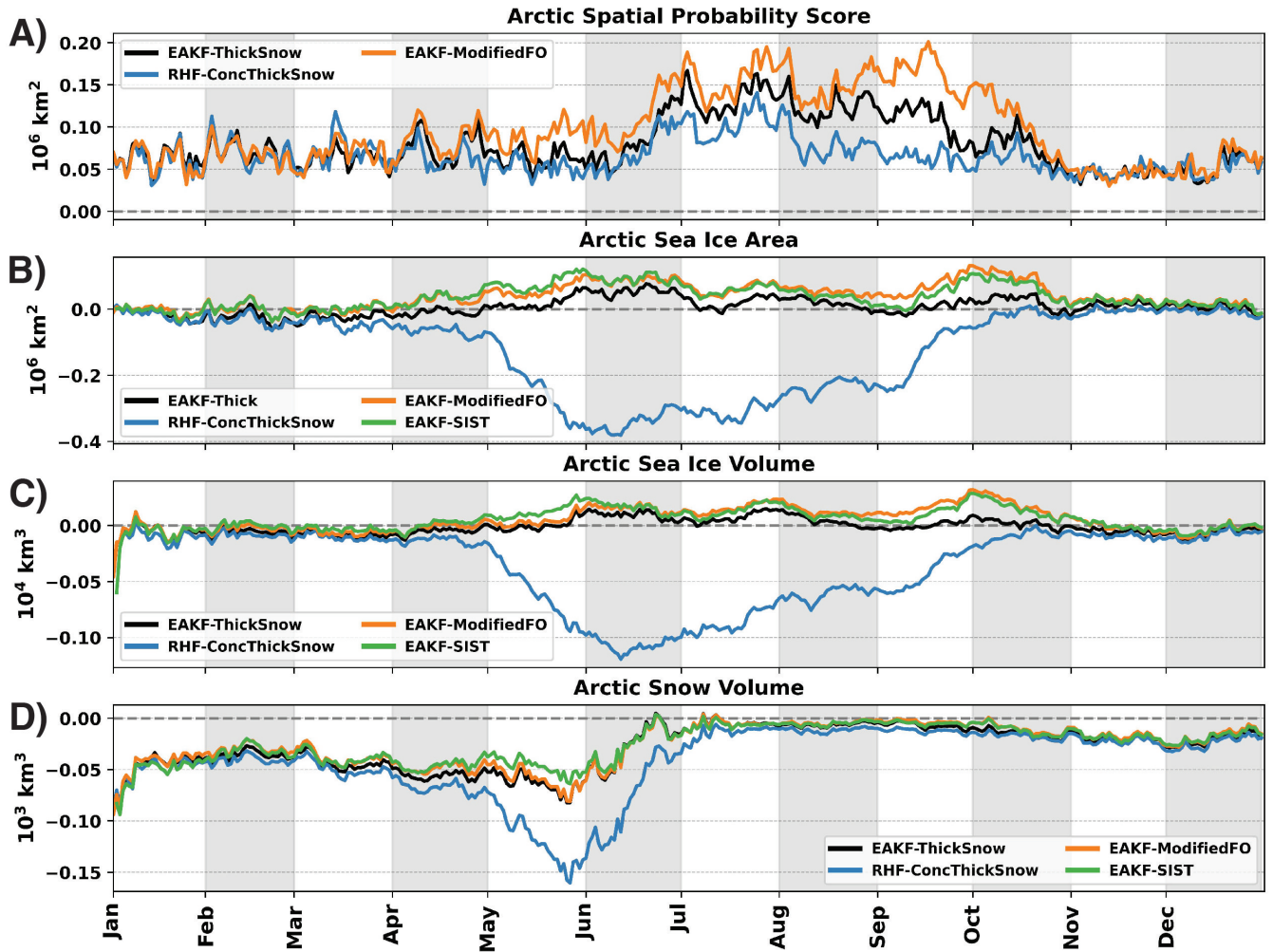


Figure 7. Same as Figure 3 but for EAKF-ThickSnow, RHF-ConcThickSnow, EAKF-ModifiedFO and EAKF-SIST.

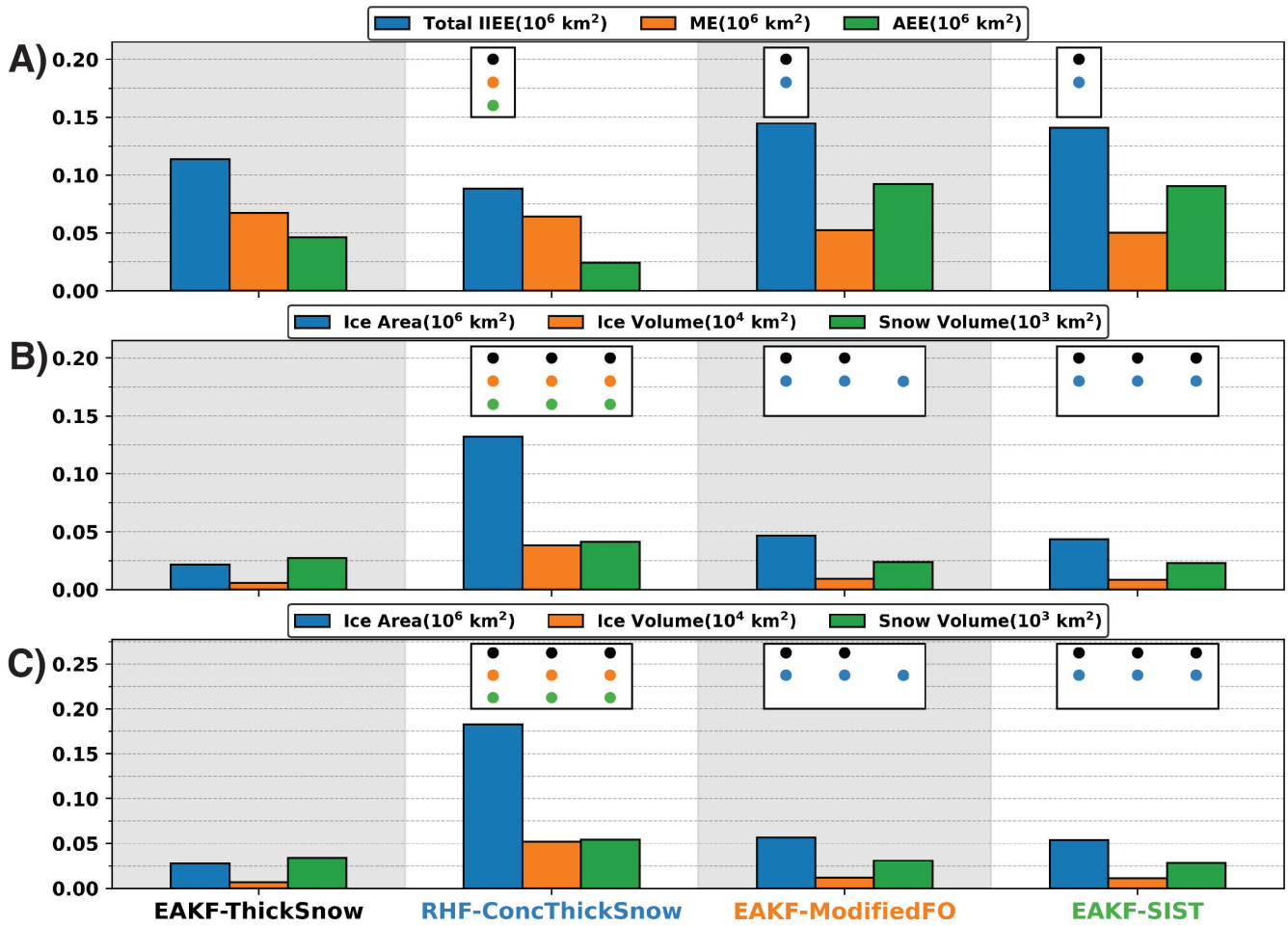


Figure 8. Same as Figure 4 but for EAKF-ThickSnow, RHF-ConcThickSnow, EAKF-ModifiedFO and EAKF-SIST

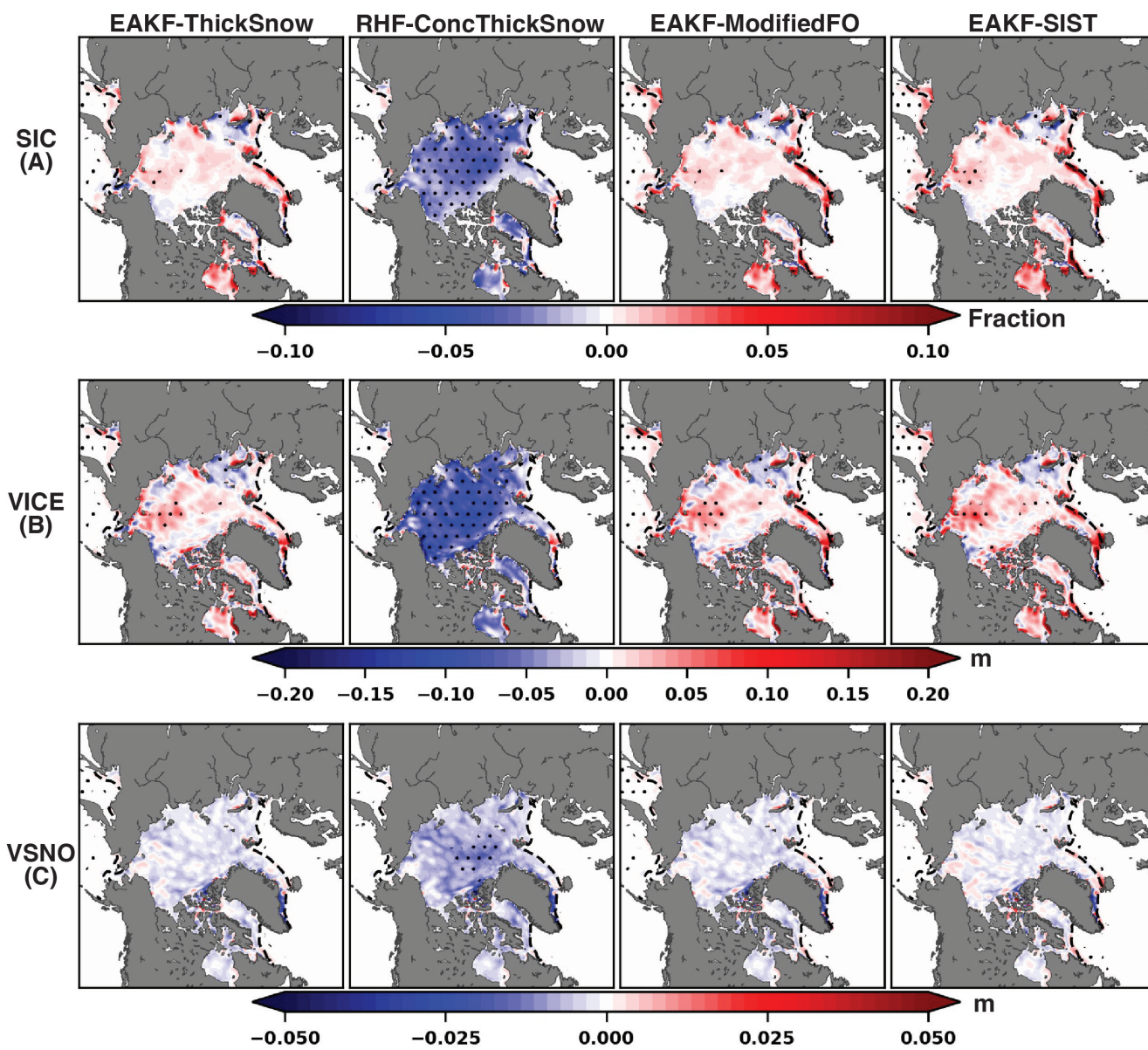


Figure 9. Same as Figure 5 but for EAKF-ThickSnow, RHF-ConcThickSnow, EAKF-ModifiedFO and EAKF-SIST.

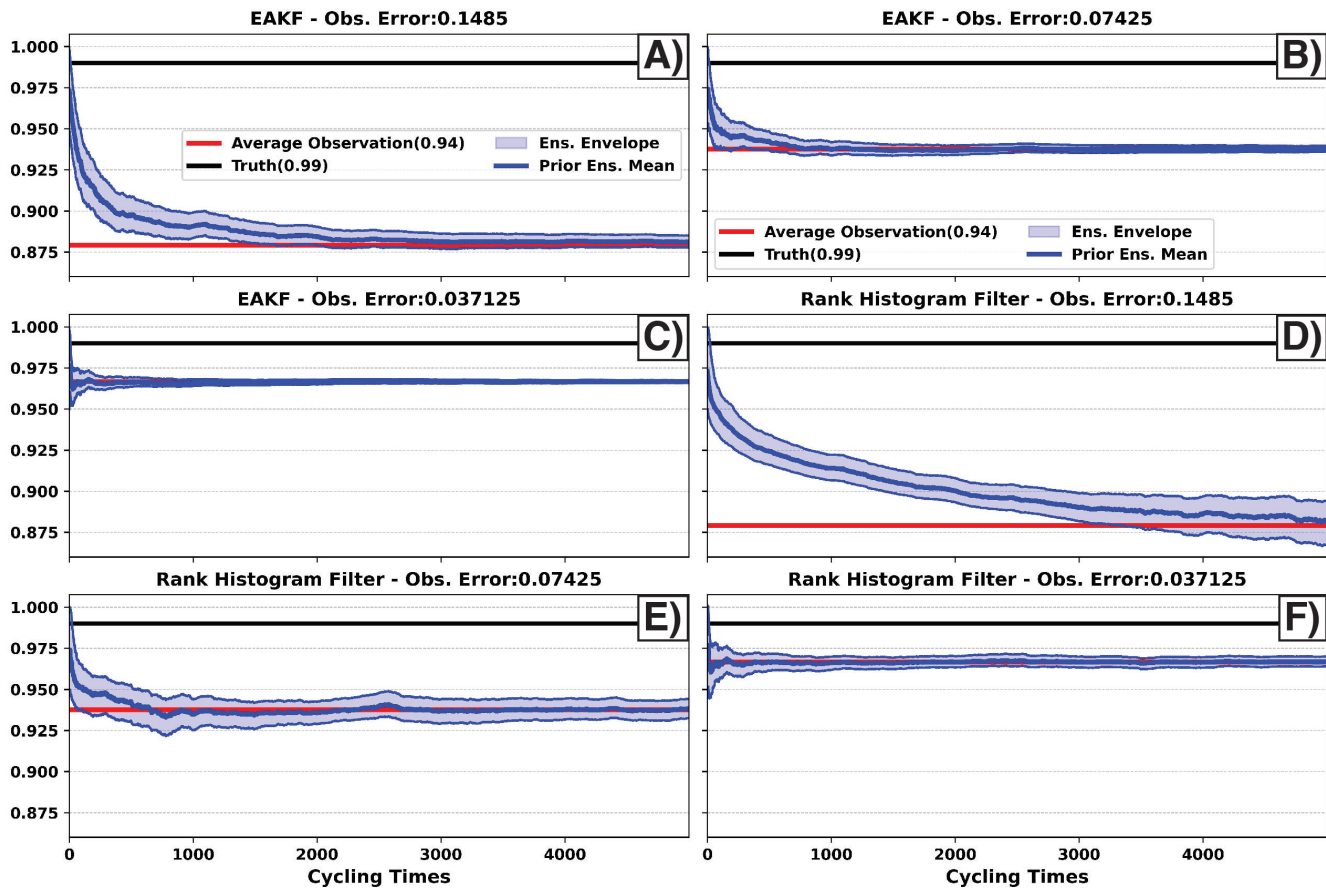


Figure 10. Prior ensemble mean (blue line) time series of SIC for experiments using (A,B,C) EAKF and (D,E,F) RHF. Each experiment was completed with observation error set to (A,D) 0.1485, (B,E) 0.07425, and (C,F) 0.037125. The red line represents the average observation value over the cycling period. The black line represents the true value over the cycling period.

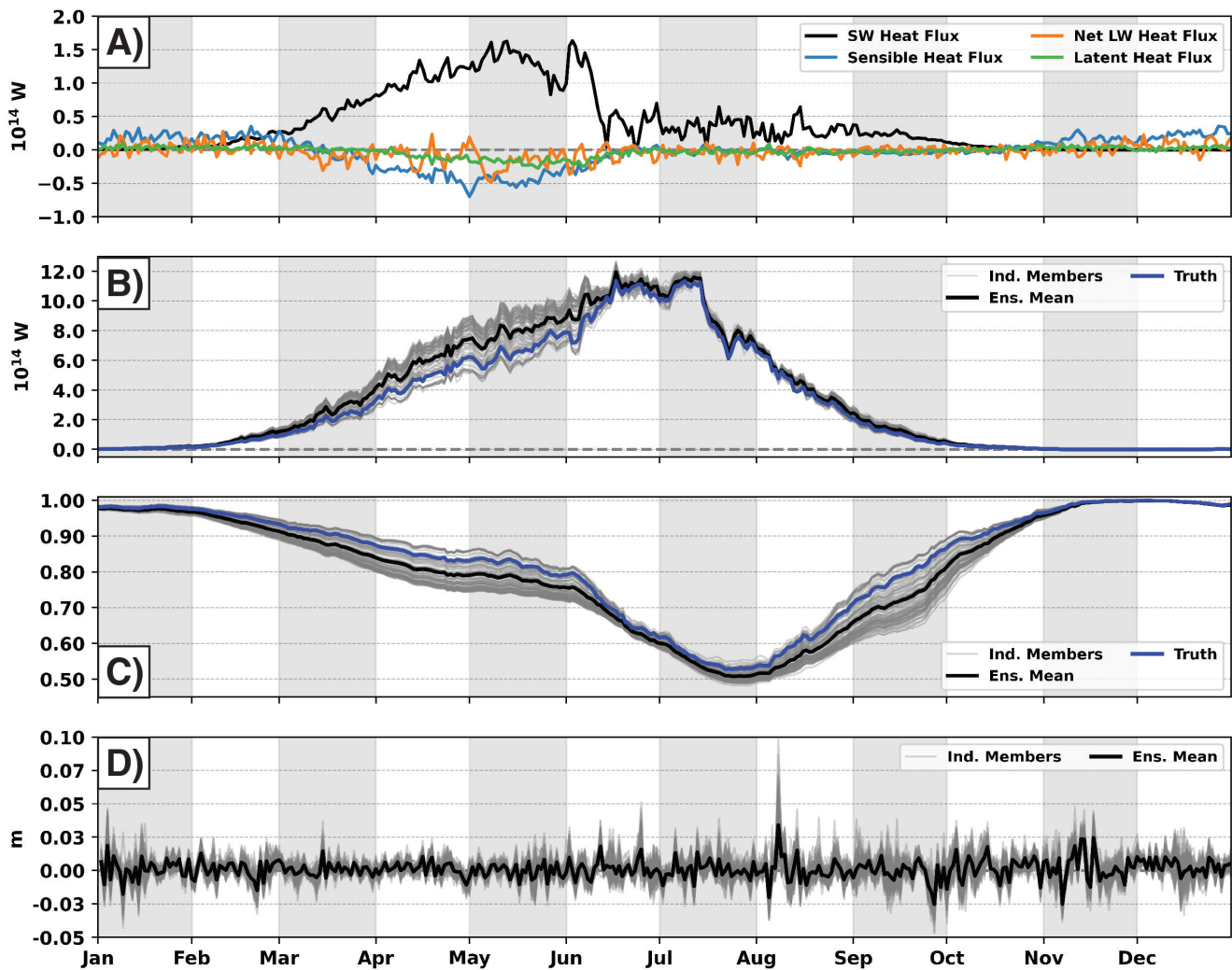


Figure 11. Panel (A): Ensemble mean daily biases of sea ice accumulated atmospheric heat fluxes for EAKF-ConcThick compared to the truth. The plotted atmospheric heat flux components include: shortwave heat flux (black line), sensible heat flux (blue line), net longwave heat flux (orange line), and latent heat flux (green line). Gray dashed line represents the zero reference line. **Panel (B):** Time series of sea ice accumulated shortwave heat flux for EAKF-ConcThick. The gray lines are the individual ensemble members, the black line is the ensemble mean, and the blue line is the truth. Gray dashed line represents the zero reference line. **Panel (C):** Same as Panel (B) but for mean surface albedo over sea ice. **Panel (D):** Daily biases of sea ice accumulated snowfall for EAKF-ConcThick compared to the truth. The gray lines are the individual ensemble members, and the black line is the ensemble mean.

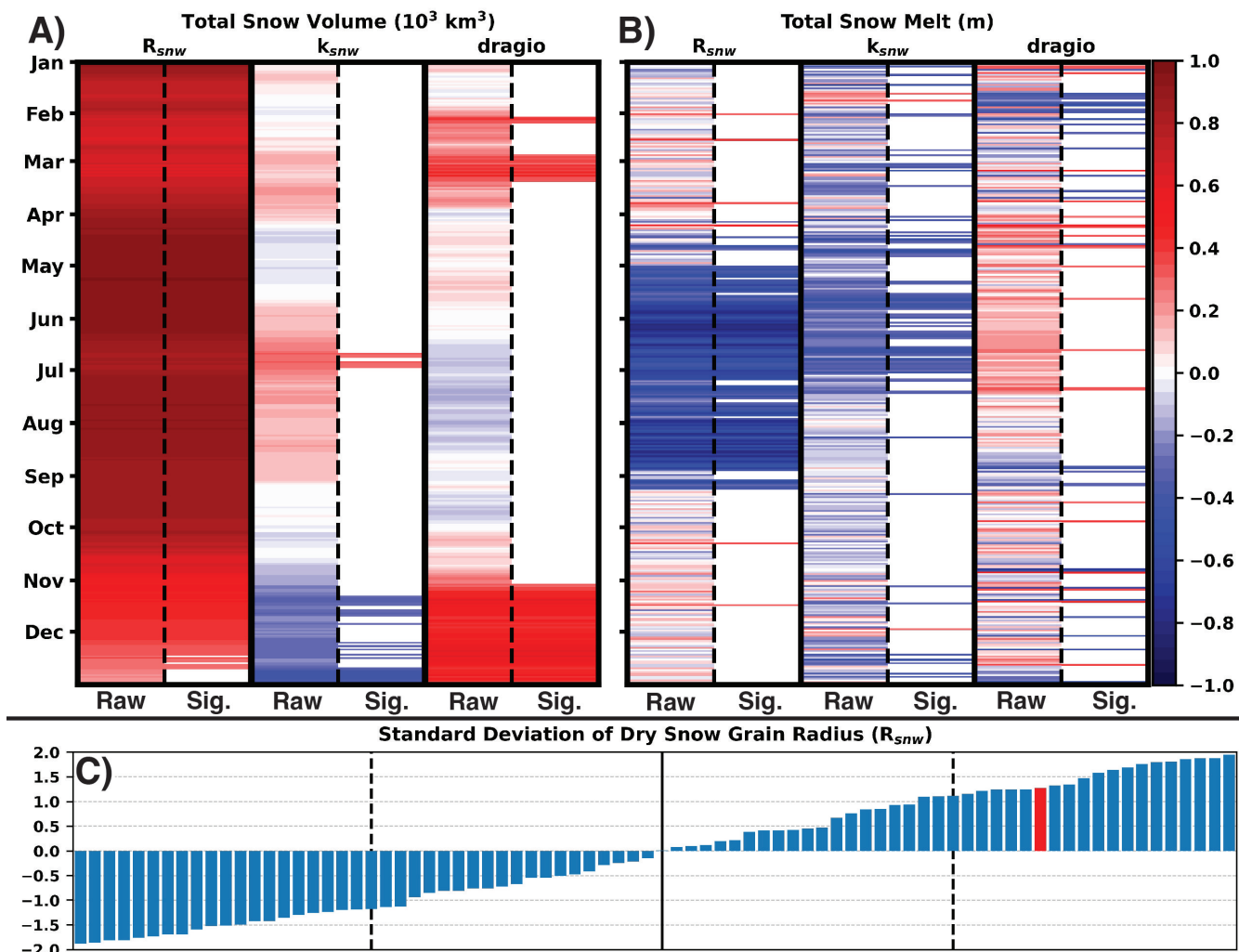


Figure 12. Panel (A): Daily correlations between perturbed CICE parameters and total snow volume over the Arctic. Correlations are computed using a Spearman's rank correlation method where both the raw correlations (**Raw**) and significant correlations with confidence at 99% (**Sig.**) are shown. **Panel (B):** Same as Panel (A) but for total snow melt over the sea ice in the Arctic. **Panel (C):** Sorted perturbed R_{snw} parameter values for each ensemble member. Red bar indicates the truth member. Black line is the median and the two dash lines represent the interquartile range.